PI31 is an adaptor protein for proteasome transport

Kai Liu[1], Sandra Jones[1], Adi Minis[1], Jose Rodriguez[1], Henrik Molina[2], Hermann Steller[1,3,*]

[1]Strang Laboratory of Apoptosis and Cancer Biology, The Rockefeller University, 1230 York Avenue, New York, NY 10065, USA.

[2]The Rockefeller University Proteomics Resource Center, The Rockefeller University, New York, NY, 10065, USA

[3]Lead contact

*Correspondence: steller@rockefeller.edu.

Summary

Protein degradation by the ubiquitin-proteasome system (UPS) is critical for neuronal function, plasticity and survival. Neurons rely on axonal transport of proteasomes to mediate protein breakdown at synapses, but how proteasomes are coupled with molecular motors and how this transport is regulated remains largely unknown. We show that the conserved proteasome-binding protein PI31 mediates axonal transport of proteasomes. PI31 directly interacts with both proteasomes and dynein light chain proteins (DYNLL1/2) and thereby serves as an adaptor to couple proteasomes with motors. Moreover, phosphorylation of PI31 at a conserved site by p38 MAPK promotes binding of PI31 to DYNLL1/2, suggesting a mechanism to regulate loading of proteasomes onto DYNLL1/2. Consistent with this model, both knockout and non-phosphorable mutants of PI31 impair proteasome movement in axons of *Drosophila* motor neurons. Because mutations affecting PI31 activity are associated with human neurodegenerative diseases, impairment of PI31-mediated axonal transport of proteasomes may be the root cause of these disorders.

Keywords: ubiquitin-proteasome system, protein degradation, PI31, microtubule-dependent transport, dynein light chain LC8-type proteins, p38 MAPK, axon, synapse, neurodegenerative diseases, *Drosophila*

Introduction

Protein homeostasis (proteostasis) is essential for cellular and organismal health (Balch et al., 2008; Glickman and Ciechanover, 2002; Goldberg, 2003; Labbadia and Morimoto, 2015; Varshavsky, 2005; Vilchez et al., 2014; Wolff et al., 2014). Eukaryotic cells have two major systems for clearing unwanted, damaged and potentially toxic proteins: the ubiquitin-proteasome system (UPS) and the autophagy-lysosome system(Bento et al., 2016; Dikic and Elazar, 2018; Glickman and Ciechanover, 2002; Goldberg, 2003; Levine and Kroemer, 2008; Murata et al., 2009; Nakatogawa et al., 2009; Schmidt and Finley, 2014). The UPS carries out the degradation of the vast majority of intracellular proteins, whereas autophagy is primarily responsible for the removal of protein aggregates and damaged organelles. In the UPS, proteins are tagged for destruction by the linkage of multiple copies of ubiquitin. The actual degradation of proteins in the UPS is carried out by multi-subunit protease particles termed 26S proteasomes(Baumeister et al., 1998; Collins and Goldberg, 2017; Glickman and Ciechanover, 2002). The 26S proteasomes consist of 20S core particles, which contain the active proteases, and 19S regulatory subunits(Collins and Goldberg, 2017; Murata et al., 2009).

It has been suggested that proteasomes are typically present in excess and that their capacity is not fully used, at least in the absence of stress(Asano et al., 2015). On the other hand, some cell types appear to require special mechanisms to position proteasomes to appropriate sub-cellular compartments where protein breakdown occurs. This is especially important for neurons, since they are very large, structurally complex and highly compartmentalized cells that require transport mechanisms to allocate proteasomes to sites distant from the cell body (Bingol and Sheng, 2011; Tai and Schuman, 2008).

Proteasome function is required for growth and pruning of both axons and dendrites during development (DiAntonio et al., 2001; Erturk et al., 2014; Kuo et al., 2005; Wan et al., 2000; Watts et al., 2003). Moreover, in mature neurons UPS-mediated protein degradation at synapses is critical for activity-dependent plasticity, learning and memory(Bingol and Sheng, 2011; Campbell and Holt, 2001; Ding et al., 2007; Hegde et al., 2014; Lee et al., 2008; Pak and Sheng, 2003; Patrick, 2006; Yi and Ehlers, 2005).

Recently, proteasomes were found to insert into the plasma membrane of neurons and acutely regulate synaptic activity and calcium signaling(Ramachandran et al., 2018; Ramachandran and Margolis, 2017). Due to the considerable distances from the soma, neurons employ microtubule-based transport mechanisms to deliver proteasomes to the periphery of neurons(Bingol and Schuman, 2006; Hsu et al., 2015; Kreko-Pierce and Eaton, 2017). However, despite the critical function of proteasomes at synapses, much remains to be learned about the underlying transport mechanisms. CamKIIα-dependent phosphorylation of the proteasome subunit Rpt6 is one mechanism to recruit proteasomes into dendritic spines, where excitatory postsynaptic densities are harbored, in response to neuronal depolarization(Bingol and Schuman, 2006; Bingol et al., 2010; Djakovic et al., 2009). This also directly links neuronal activity with local proteasome regulation, since CamKIIα can be activated by calcium entry through NMDA receptors in depolarized neurons. On the other hand, the mechanisms regulating proteasome transport in axons and their localization to the presynaptic regions are less clear. One of the molecular motors, the dynein complex, plays a key role in motility of proteasomes in axons(Hsu et al., 2015; Kreko-Pierce and Eaton, 2017). A recent study identified dynein light chain LC8-type proteins (DYNLL1/2) as components of microtubule-dependent proteasome transport in *Drosophila* neurons (Kreko-Pierce and Eaton, 2017). However, the central unresolved questions are how exactly proteasomes are coupled to microtubule-based motor complexes and how proteasome transport is coordinated with cellular/sub-cellular status to appropriately distribute the protein degradation machineries.

Here we show that the conserved proteasome-binding protein PI31 ("proteasome inhibitor of 31kD") mediates fast axonal transport of proteasomes in *Drosophila* motor neurons by acting as an adapter between proteasomes and dynein light chain LC8-type proteins (DYNLL1/2). Moreover, a conserved phosphorylation site on PI31 was identified as a molecular switch that regulates the interaction between PI31 and dDYNLL1/2, and controls proteasome transport in axons. PI31 was originally identified based on its ability to inhibit 20S-mediated hydrolysis of peptides *in vitro* (Chu-Ping et al., 1992; McCutchen-Maloney et al., 2000; Zaiss et al., 1999). On the other hand, our work showed that inactivation of PI31 impairs protein degradation during sperm

maturation in *Drosophila*, and that PI31 can stimulate the proteolytic capacity of cells by promoting the assembly of 19S and 20S particles into the fully active 26S proteasomes(Bader et al., 2011; Cho-Park and Steller, 2013). Similarly, the PI31 ortholog in yeast, Fub1, is required to alleviate proteotoxic stress (Yashiroda et al., 2015). However, studies in cultured HEK293 cells have failed to reveal a clear effect of PI31 for proteasome activity, suggesting that PI31 function may be different in different cell types and systems (Li et al., 2014).

PI31 also binds directly and strongly to the F-box protein Ntc/FBXO7/PARK15, and this interaction is conserved from *Drosophila* to mammals(Bader et al., 2011; Kirk et al., 2008). Interestingly, mutations in *FBXO7/PARK15* impair proteasome function and cause a juvenile form of Parkinson's Disease (PD) in humans and PD-like symptoms in mice(Conedera et al., 2016; Di Fonzo et al., 2009; Paisan-Ruiz et al., 2010; Vingill et al., 2016). Since many age-related neurodegenerative diseases, including Alzheimer's Disease (AD) and PD, are characterized by the accumulation of protein aggregates, it is possible that mutations in *FBXO7/PARK15* impair the clearance of pathological proteins (Ballatore et al., 2007; Irvine et al., 2008; Li and Li, 2011; Oddo, 2008; Ross and Poirier, 2004; Tai and Schuman, 2008). F-box proteins serve as substrate recognition modules in multi-component E3-ligase complexes for UPS-mediated protein degradation (Bai et al., 1996; Kipreos and Pagano, 2000; Skaar et al., 2013; Skowyra et al., 1997). However, very unexpectedly for an E3 ligase, binding of FBXO7 to PI31 does not result in PI31 degradation but rather serves to protect PI31 from proteolytic cleavage (Bader et al., 2011; Vingill et al., 2016). These observations are consistent with the idea that loss of *FBXO7* leads to impaired proteasome function through inactivation of PI31, but direct evidence for this model is lacking due to insufficient knowledge about the precise function of PI31 in neurons. Moreover, PI31 was linked to Alzheimer's disease (AD) by a genome-wide association study, and mutations in another PI31-interacting protein, Valosin-Containing Protein (VCP/P97), cause amyotrophic lateral sclerosis (ALS) (Clemen et al., 2015; Johnson et al., 2010; Sherva et al., 2011). These findings raise the interesting possibility that PI31 has a critical function in neurons.

In order to address the function of PI31 in neurons, we investigated the consequences of PI31 inactivation in *Drosophila* motor neurons. We found a striking requirement of PI31 for synaptic structure and function. Loss of PI31 function altered the structure of presynaptic active zones and caused defects in protein homeostasis in the periphery of neurons. Significantly, we identified *Drosophila* homologs of dynein light chain LC8-type proteins (dDYNLL1/Ctp and dDYNLL2/Cdlc2) as binding partners of PI31. PI31 can directly interact with both dDYNLL1/Ctp and proteasomes *in vitro*, and it can promote binding of proteasomes to dDYNLL1/Ctp. Importantly, inactivation of PI31 blocks proteasome motility in axons, similar to inactivation of dDYNLL1/Ctp (Kreko-Pierce and Eaton, 2017). We conclude that PI31 is a direct adaptor protein to load proteasomes onto dynein complexes and thereby mediates axonal transport of proteasomes. The interaction of PI31 and DYNLL1/2 is conserved from *Drosophila* to mammals, indicating that this function is conserved. Moreover, we identified a conserved phosphorylation site in PI31 that is critical for binding to DYNLL1/2. Mutating this site impaired proteasome movement in axons of *Drosophila* motor neurons, suggesting that phosphorylation promotes loading of proteasome to DYNLL1/2. Finally, we found that the stress-activated kinase p38 MAPK is responsible for phosphorylation of PI31. Collectively, these results suggest a molecular link between cellular stress and proteasome transport. Because mutations affecting PI31 activity and the misregulation of p38 MAPK are both associated with human neurodegenerative diseases, impairment of PI31-mediated axonal transport of proteasomes may be the root cause of these disorders.

Results

Requirement of PI31 for neuronal function and synaptic structure

PI31 is a conserved proteasome-binding protein, and its expression is enriched in heads and testes in *Drosophila* (Bader et al., 2011; Chintapalli et al., 2007; Cho-Park and Steller, 2013; McCutchen-Maloney et al., 2000; Yashiroda et al., 2015). Moreover, mutations affecting PI31 and its interaction proteins were associated with neurodegenerative diseases in human(Conedera et al., 2016; Di Fonzo et al., 2009; Johnson et al., 2010; Koppers et al., 2012; Paisan-Ruiz et al., 2010; Sherva et al., 2011).

These findings imply that the function of PI31 is crucial for neurons. To study the role of PI31 in neurons, we used the *R94G06-GAL4* to drive the expression of *UAS-HA-PI31*, and examined its localization in neurons. *R94G06-GAL4* overcomes the non-specific expression in sensory neurons of other GAL4 drivers, allowing for highly specific expression in one motor neuron (MN1-IB) in the ventral nerve cord of each larval hemi-segment, the axon of which targets Muscle 1 (Figure S1A)(Sanyal, 2009). We found that PI31 forms puncta along axons and at neuromuscular junctions (NMJs) (Figure 1A), suggesting it may have a local function there.

Local activity of proteasomes plays a key role in turnover of synaptic proteins and regulates the growth, strength, activity and plasticity of synapses (Bingol and Schuman, 2006; DiAntonio et al., 2001; Ding et al., 2007; Djakovic et al., 2009; Ehlers, 2003; Erturk et al., 2014; Hegde et al., 2014; Kuo et al., 2005; Speese et al., 2003; Willeumier et al., 2006). As a proteasome-binding protein that forms puncta in axons and NMJs, PI31 may promote local protein degradation there. To study this possibility, we conducted immunofluorescence studies to compare the amounts of poly-ubiquitinated proteins (Poly-Ub), the substrates of proteasomes, in axons and at NMJs of wild-type and *PI31*$^{-/-}$ larvae. Quantification of these results demonstrates that *PI31*$^{-/-}$ larval axons contained significantly more Poly-Ub puncta compared to wild-type axons (Figure 1B and 1C). Consistently, the intensity of Poly-Ub staining at Muscle 4 (M4) NMJs was also elevated (Figure 1D and 1E). These data indicate that the loss of PI31 impairs protein degradation in axons and synapses, and they suggest that PI31 has a critical role in regulating proteasome abundance or activity in nerve terminals.

Since local activity of UPS is important for the growth and maintenance of NMJs, we examined NMJ anatomy of wild-type and *PI31*$^{-/-}$ larvae(DiAntonio et al., 2001; Valakh et al., 2012; Wan et al., 2000). For this purpose, we conducted immunofluorescence analyses using anti-Horseradish peroxidase (HRP) and Bruchpilot (BRP) antibodies, and analyzed M4 NMJs (Figure S1B and 1F) and Muscle 6/7 (M6/7) NMJs (Figure S1C and S1D). The anti-HRP antibody binds to neuronal membranes and serves as a marker for neuronal morphology(Jan and Jan, 1982). BRP is a core scaffold

protein for presynaptic active zone (AZ). It has homology to the human AZ protein ELKS/CAST/ERC and is crucial for AZ assembly, proper clustering of Ca2+ channels within AZs, and efficient neurotransmitter release. It is widely used as a marker for proper presynaptic AZ assembly(Kittel et al., 2006; Sigrist, 2009; Wagh et al., 2006). Although the overall morphology of NMJs was similar between wild-type and *PI31*$^{-/-}$ larvae (Figure S1B and S1C), the number of Brp puncta was significantly reduced in *PI31*$^{-/-}$ larvae (Figure 1F, 1G, and S1D), suggesting a defect of AZ assembly. In particular, we found that the number of small-volume Brp puncta (<0.5 μm^3) was dramatically reduced in *PI31*$^{-/-}$ larvae, whereas big-volume ones (>0.5 μm^3) appeared not affected (Figure 1H). Our results indicate that PI31 is required to maintain proper synaptic morphology at NMJ.

To examine whether the synaptic defect reflects a cell autonomous requirement for PI31, we used the mosaic analysis with a repressible cell marker (MARCM) to inactivate PI31 in a limited number of cells (Wu and Luo, 2006) (Figure S1E and 1I). *PI31*$^{-/-}$ neurons are marked by GFP expression, whereas GFP-negative neurons are *PI31*$^{+/-}$ and serve as an internal control. Quantitative results indicated that *PI31*$^{-/-}$ neurons have reduced number of Brp puncta (Figure 1I and 1J). This is consistent with the results from PI31 full knockout larvae (Figure 1F, 1G and S1D), and suggests that the synaptic defect is a cell autonomous phenotype. Interestingly, using a GluRIIC antibody that labels postsynaptic densities to co-stain MARCM M4 NMJs with Brp antibody, we found that some synapses in *PI31*$^{-/-}$ neurons lost Brp puncta but maintained postsynaptic densities (Figure 1K and 1L, indicated by white arrowheads). A previous report demonstrated that knockdown of proteasome subunits in motor neurons results in similar changes of synapses, suggesting that the synaptic defects of *PI31*$^{-/-}$ neurons are due to insufficient proteasome activity in synapses(Valakh et al., 2012).

We also inactivated PI31 in neurons with a neuron-specific driver, *Nrv2-GAL4*(Sun et al., 1999). *Nrv2>PI31 RNAi* homozygotes died as pharate adults that appeared overall well-developed. These mutants initiated but did not complete the eclosion process as they displayed a strong leg motor defect that made it impossible for

them to escape from pupal cases (Table S1). Taken together, these results indicate that inactivation of PI31 leads to the impairment of protein degradation in axons and synapses, which causes structural and functional synaptic defects.

Dynein light chain LC8-type proteins are binding partners of PI31

To understand the mechanism by which PI31 promotes proteostasis in the periphery of neurons, we looked for new binding partners of PI31. For this purpose, we expressed N-terminal HA-tagged PI31 (HA-PI31) in flies and performed anti-HA co-immunoprecipitation (Co-IP) followed by label-free quantitative mass spectrometry (MS). Since HA-PI31 rescued the lethality of PI31 knockout flies, we conclude that the N-terminal tag did not interfere with PI31 functions(Bader et al., 2011). Results from this analysis revealed that all 20S proteasome subunits were highly enriched in the ani-HA-PI31 Co-IP, compared to the control Co-IP, which did not include HA-PI31 (Figure 2A). This is consistent with previous studies, and suggests our co-IP-MS method reflects the interactome of PI31 *in vivo*(Bader et al., 2011; Cho-Park and Steller, 2013; McCutchen-Maloney et al., 2000; Yashiroda et al., 2015).

Interestingly, among the statistically most significant proteins, we noticed two dynein light chain LC8-type proteins, Ctp (*Drosophila* homolog of dynein light chain LC8-type 1, dDYNLL1) and Cdlc2 (*Drosophila* homolog of dynein light chain LC8-type 2, dDYNLL2) (Figure 2A). Both proteins consist of 89 amino acids, share 98.9% identity, and differ in only one amino acid (Figure S2A). Since both unique peptides were identified by MS, this suggests that both proteins can bind to PI31 (Figure S2B). Dynein proteins are microtubule-dependent molecular motors that are responsible for fast intracellular transport of various cargos (Hirokawa et al., 2010; Reck-Peterson et al., 2018; Schliwa and Woehlke, 2003; Vale, 2003). Interestingly, dDYNLL1/Ctp was recently shown to mediate axonal transport of proteasomes in *Drosophila* motor neurons(Kreko-Pierce and Eaton, 2017). Our results raise the possibility that PI31 regulates proteasome transport in axons.

In order to further study the interaction between PI31 and dDYNLL1/2, we conducted Co-IP-Western blot assays. HA-PI31 was able to pull down dDYNLL1/2 in both S2 cells and transgenic flies (Figure S2C and 2B), indicating the existence of a PI31-dDYNLL1/2 complex *in vivo*. To avoid possible overexpression artifacts and examine the interaction of PI31 and dDYNLL1 under endogenous expression levels, we generated a *HA-PI31*$^{Knock\text{-}in}$ fly strain through inserting a HA-tag into the N-terminus of the genomic locus of PI31 in frame with its coding sequence by CRISPR-Homology Directed Repair (HDR) (Port et al., 2014). The expression level of HA-PI31$^{\text{Knock-in}}$ was comparable to PI31 levels in wild-type flies (Figure 2C). Using this system to conduct anti-HA Co-IP experiments, we were able to show that PI31 can pull down dDYNLL1/2 and proteasomes at physiological levels of protein expression (Figure 2C). To provide additional evidence for the interaction of PI31 and dDYNLL1/2, we also performed the reciprocal Co-IP using FLAG-dDYNLL1 as the bait and found it to successfully pull down PI31 (Figure 2D).

Dynein motor complexes are highly conserved in evolution(Hirokawa et al., 2010; Reck-Peterson et al., 2018; Schliwa and Woehlke, 2003; Vale, 2003). In order to investigate whether the interaction between PI31 and dynein light chain LC8-type proteins is conserved in mammals, we performed Co-IP experiments in both MEFs and HEK293 cells. Using GFP-tagged mouse PI31 (GFP-mPI31) and HA-tagged human PI31 (HA-hPI31), we found that PI31 interacted with DYNLL1/2 in both cell types (Figure 2E and S2D). Taken together, these findings indicate that PI31 interacts with DYNLL1/2 proteins, and that this interaction is conserved from *Drosophila* to mammals.

Previous work showed that PI31 binds directly to 20S proteasomes (Bader et al., 2011; Cho-Park and Steller, 2013; Chu-Ping et al., 1992; McCutchen-Maloney et al., 2000; Yashiroda et al., 2015). This is consistent with our Co-IP-MS results that mainly identified 20S proteasome subunits as binding partners of PI31, but did not detect 19S proteasome subunits significantly (Figure 2A). However, this does not mean that PI31 is only in a complex with 20S proteasomes but not with 26S proteasomes, since we did not include ATP to preserve the stability of 26S particles(Liu et al., 2006). To study whether

PI31 can form a complex with 26S proteasomes, we used again *HA-PI31*$^{Knock\text{-}in}$ flies. This time, anti-HA Co-IP experiments were conducted in the presence of ATP to preserve 26S proteasomes, and interacting proteins were eluted under native conditions and analyzed by native gel assays. Our results indicate that PI31 interacts with both 20S proteasomes and single-capped 26S proteasomes *in vivo* (Figure S3). On the other hand, double-capped 26S proteasomes were not captured by this approach, suggesting that PI31 cannot bind to them efficiently (Figure S3). Based on these results, it is possible that PI31 is involved in the transport of both 20S and single-capped 26S proteasomes.

A conserved phosphorylation event is important for the interaction of PI31 with dDYNLL1/2

Analysis of Co-IP-MS results revealed that *Drosophila* PI31 is phosphorylated at Serine 168 (Figure 3A). The corresponding site in human PI31 (Serine 153) is also phosphorylated, indicating that this modification is conserved from flies to human (Figure 3B and 3C). To study the function of this phosphorylation, we generated transgenic fly strains expressing a non-phosphorable mutant of *Drosophila* PI31 (Serine 168 to Alanine mutant, S168A) and compared its interactome with the interactome of wild-type PI31. Significantly, we identified dDYNLL1/2 as the most prominently affected binding partner of PI31 (Figure 3D). This result suggests that S168 phosphorylation promotes binding of PI31 to dDYNLL1/2.

PI31 phosphorylation promotes direct binding to dDYNLL1/2

To investigate the role of phosphorylation in the interaction of PI31 and dDYNLL1/2 in more details, we first conducted Co-IP-Western Blot assays. These results indicate that dDYNLL1/2 can efficiently interact with wild-type and phospho-mimetic PI31 (Serine 168 to Aspartic acid mutant, S168D) in both S2 cells and transgenic flies. In contrast, this interaction was significantly reduced for the non-phosphorable mutant of PI31(S168A) (Figure 4A and B). The importance of phosphorylation was further confirmed by a reciprocal Co-IP using FLAG-dDYNLL1 as the bait (Figure 4C). Because a significant fraction of HA-PI31 is phosphorylated in

Drosophila, the phospho-mimetic mutant of PI31 (S168D) did not significantly increase the interaction between PI31 and dDYNLL1/2.

Next, we investigated whether PI31 and dDYNLL1/Ctp interact directly with each other, and whether phosphorylation promotes interaction *in vitro*. For this purpose, we expressed recombinant GST tagged wild-type (GST-PI31-WT), non-phosphorable mutant (GST-PI31-S168A), two phospho-mimetic mutants (GST-PI31-S168D and GST-PI31-S168E), and FLAG-dDYNLL1 in *E. coli.* These various recombinant PI31 proteins were used for GST-pull down assays. The results revealed that GST-PI31-WT can interact with FLAG-dDYNLL1, whereas GST alone can not (Figure 4D). Importantly, binding was dramatically enhanced by the two phospho-mimetic mutants (GST-PI31-S168D and GST-PI31-S168E), whereas the non-phosphorable mutant (GST-PI31-S168A) had no activity (Figure 4D). We conclude that PI31 is a direct binding partner of dDYNLL1/Ctp, and that phosphorylation of PI31 stimulates binding.

PI31 promotes the formation of dDYNLL1/Ctp-proteasome complex

Since PI31 can directly bind to both dDYNLL1/Ctp and proteasomes, we explored the idea that this protein may serve as an adapter to promote formation of a multi-protein complex containing proteasome and dynein. In order to look for evidence of such a complex, we expressed FLAG-dDYNLL1 in S2 cells and conducted anti-FLAG Co-IP experiments to see if proteasomes can be pulled down. Through MS analysis, we identified most of the 20S proteasome subunits (Figure 5A). This indicated the existence of a dDYNLL1/Ctp-proteasome complex. Interestingly, PI31 was among the statistically most significant binding partners of dDYNLL1/Ctp, providing additional support for the relevance of this interaction. We further validated the existence of a dDYNLL1/Ctp-proteasome complex by Co-IP-Western blot assays using an antibody toward the 20S proteasome subunit α7 (Figure 5B).

If PI31 is an adaptor protein mediating the formation of dDYNLL1/Ctp-proteasome complexes, increased amounts of PI31 should facilitate complex formation. To test this possibility, we expressed FLAG-dDYNLL1 with different forms of HA-PI31 in S2 cells, performed anti-FLAG Co-IP experiments, and compared the amount of

proteasomes pulled down by FLAG-dDYNLL1. These experiments demonstrate that elevated levels of PI31 can indeed increase the amount of proteasomes bound to dDYNLL1/Ctp (Figure 6A). Interestingly, the non-phosphorable mutant of PI31 (S168A) largely lost this ability (Figure 6A).

To test whether this effect is due to direct interactions mediated by PI31, we reconstituted the complex *in vitro* using purified 20S proteasomes and recombinant GST-PI31 and FLAG-dDYNLL1 expressed in *E.coli*. Firstly, FLAG-dDYNLL1 was bound to anti-FLAG-magnetic beads. Then, 20S proteasomes were added alone, with GST, or with GST tagged wild-type or mutant PI31 proteins. This approach showed that GST-PI31 was able to load 20S proteasomes onto dDYNLL1/Ctp, whereas 20S proteasomes alone or with GST did not bind to dDYNLL1/Ctp (Figure 6B). Importantly, the two phosphor-mimetic mutants (GST-PI31-S168D and GST-PI31-S168E) showed stronger ability than wild-type (GST-PI31-WT) or the non-phosphorable mutant (GST-PI31-S168A) to load proteasomes onto the dDYNLL1/Ctp (Figure 6B). Taken together, these results show that PI31 is a direct adaptor protein that promotes the formation of a complex between proteasomes and dDYNLL1/Ctp, and this ability is enhanced by its phosphorylation.

PI31 is required for the axonal transport of proteasomes in motor neurons

Our results so far suggest that PI31 may mediate axonal transport of proteasomes by promoting the formation of DYNLL1/2-proteasome complexes. To examine a requirement of PI31 for this process, we conducted live-imaging of proteasome movement in axons using a proteasome reporter UAS-Prosβ5-RFP, which is incorporated into functional proteasomes when expressed in motor neurons(Kreko-Pierce and Eaton, 2017). For these studies, the reporter was driven by *R94G06-GAL4* to ensure the specificity of its expression in motor neurons, which is important for the determination of transport directions (Figure S1A). Using this assay, we found that inactivation of PI31 significantly reduced motility of axonal proteasomes (Figure 7A and 7B, and Movie S1 and S2). In wild-type larva, 30.5% of proteasome particles exhibited anterograde movement with an average velocity of 0.71±0.06 μm/s; 44.1% of proteasome particles exhibited retrograde movement with an average velocity of 0.42±0.03 μm/s; 22.6% of

proteasome particles appeared stationary; and the remaining 2.8% of proteasome particles moved reversely during the live imaging (Figure 7A and 7B, and Movie S1).

Next, we examined the movement of proteasome particles in *PI31*$^{-/-}$ larva. In this case, both anterograde and retrograde movement of proteasomes was severely reduced: 78.5% of proteasome particles remained stationary, and only 8.2% and 10.6% of proteasome particles displayed anterograde and retrograde movement, respectively (Figure 7A and 7B, and Movie S2). These phenotypes recapitulate the defects of proteasome transport reported in *dDYNLL1/ctp*$^{-/-}$ motor neurons, supporting that they function in the same protein complex (Kreko-Pierce and Eaton, 2017). Together, these results indicate that PI31 is required for proteasome transport along motor neuron axons.

Our biochemical data demonstrate that S168 phosphorylation of PI31 is important for interaction with dDYNLL1 and enhances loading of proteasomes onto dDYNLL1/Ctp. To examine the functional importance of PI31-phosphorylation for proteasome transport, we generated a *PI31*^{S168A} *knock-in* fly strain in which the wild-type PI31 gene was replaced with the non-phosphorable mutant by CRISPR-Homology Directed Repair (HDR)(Port et al., 2014) (Figure S4A-C). Next, we conducted live imaging analysis of Prosβ5-RFP in homozygous *PI31*^{S168A} *knock-in* larvae. Interestingly, we found no significant effect of this mutant on anterograde and stationary proteasome particles. However, retrograde movement of proteasome particles was significantly reduced, and we also saw a dramatic increase in the number of randomly moving particles (Figure 7A, indicated by red asterisks, and Figure 7B, and Movie S3). These results indicate that the PI31 phosphorylation is important to maintain the processivity of the retrograde proteasome transport.

Since PI31 interacts with proteasomes and dynein light chain LC8-type proteins in both *Drosophila* and mammals, we explored the possibility that the function of PI31 as an adapter to mediate axonal transport of proteasomes is conserved in evolution. As a first step, we examined the subcellular localization of PI31 and proteasomes in axons of cultured mouse dorsal root ganglion (DRG) neurons. For this purpose, we transfected primary DRG neuron cultures with mouse proteasome subunit α4-mCherry and mCerulean-mPI31 and conducted live-imaging analyses (Movie S4). The results of these

experiments show that α4-mCherry and mCerulean-mPI31 co-localize and move together along DRG axons (Figure 7C and 7D, and Movie S4). These observations are consistent with the idea that the function of PI31 as an adapter to mediate axonal transport of proteasomes has been conserved to mammals.

p38 MAPK can phosphorylate PI31

Our biochemical and live imaging results demonstrate that phosphorylation of PI31 is crucial for interaction with dDYNLL1, formation of proteasome-dDYNLL1 complexes, and proteasome movement in axons. In order to identify the kinase responsible for PI31 phosphorylation, we conducted a candidate-based screen of kinase RNAi transgenic fly strains. The conserved PI31 phosphorylation site (pSerine-Proline) pointed to Proline-directed kinases, such as cyclin-dependent kinases (CDKs) and mitogen-activated protein kinases (MAPKs) (Wagih et al., 2016; Zhu et al., 2005). Therefore, we screened all available CDK and MAPK RNAi fly strains (Ni et al., 2008). Quantitative MS results indicated that knockdown of p38β MAPK reduced PI31 phosphorylation by almost 50% (Figure 8A), suggesting it as a candidate kinase responsible for PI31 phosphorylation.

p38 MAPKs can be activated by a wide range of cellular stresses as well as inflammatory cytokines(Cuenda and Rousseau, 2007; Zarubin and Han, 2005). One classical stress to activate p38 is sorbitol-induced osmotic stress(Cuenda and Rousseau, 2007; Han et al., 1994; Zarubin and Han, 2005). Therefore, we asked whether PI31 phosphorylation is elevated in response to osmotic stress. First, we generated a phosphorylation-specific antibody for Serine 153 of hPI31 (Figure S5A) and verified its specificity (Figure S5B). Next, we treated the HEK293 cells with sorbitol and assessed S153 phosphorylation of endogenous PI31. This revealed that pS153 levels were indeed elevated after the treatment, suggesting that stress promotes phosphorylation of PI31 at S153 (Figure 8B). To test whether this stress-induced phosphorylation depends on p38 MAPK, we used several distinct p38 MAPK inhibitors. Inhibition of p38α and p38β had only minor effects, but using an inhibitor targeting all four isoforms of p38 MAPK dramatically reduced S153 phosphorylation of PI31 (Figure 8C). This suggests that multiple isoforms of p38 MAPK can phosphorylate PI31. Consistently, when we used

purified recombinant p38 MAPKs and hPI31 to conduct *in vitro* kinase assays, we found that all four isoforms of p38 MAPK can directly phosphorylate PI31 (Figure 8D). We conclude that p38 MAPKs can promote phosphorylation of PI31 in response to stress.

Discussion

The degradation of unwanted and potentially toxic protein by the ubiquitin-proteasome system (UPS) is of critical importance for protein homeostasis. In addition, UPS-mediated protein degradation also sculpts cell shape during development and modifies tissues throughout life. Examples include the terminal differentiation of spermatids, loss of muscle mass in response to starvation, dendritic pruning of nerve cells, and the maturation and modification of synapses to mediate neuronal plasticity(Bader et al., 2011; Campbell and Holt, 2001; Hegde et al., 2014; Lecker et al., 1999; Lee et al., 2008; Pak and Sheng, 2003; Patrick, 2006; Qian et al., 2013; Sandri, 2013; Watts et al., 2003; Yi and Ehlers, 2005; Zhong and Belote, 2007). Neurons pose a particular challenge for regulated protein degradation due to their large size and highly compartmentalized structure. Localized regulation of UPS activity is crucial for synaptic growth, function and plasticity, and remodeling of axons and dendrites (Bingol and Schuman, 2006; DiAntonio et al., 2001; Djakovic et al., 2012; Ehlers, 2003; Erturk et al., 2014; Hamilton and Zito, 2013; Kuo et al., 2005; Pak and Sheng, 2003; Ramachandran and Margolis, 2017; Speese et al., 2003; Wan et al., 2000; Watts et al., 2003; Zhao et al., 2003). Nerve cells employ microtubule-based transport mechanisms to quickly distribute proteasomes between soma and neurites (Bingol and Schuman, 2006; Hsu et al., 2015; Kreko-Pierce and Eaton, 2017; Otero et al., 2014). Recent reports suggested that dynein complexes, especially the dynein light chain LC8-type proteins (DYNLL1/2), are important components of microtubule-dependent proteasome transport in neurons(Hsu et al., 2015; Kreko-Pierce and Eaton, 2017). However, a central unresolved question is how proteasomes are coupled to microtubule-based motor complexes, and how this process is regulated to meet dynamic demands of local protein degradation. Advances in this area are important since they provide the foundation for specific manipulation of proteasome transport, including to potentially boost clearance of toxic proteins in the periphery of neurons.

In this study, we identified dynein light chain LC8-type proteins (DYNLL1/2) as direct binding partners of the conserved proteasome regulator PI31 ("Proteasome Inhibitor of 31kD"). Since PI31 also binds directly to proteasomes, this raised the possibility that PI31 serves as an adapter to couple proteasomes via dynein light chain proteins to microtubule-based motors(Bader et al., 2011; Cho-Park and Steller, 2013; Chu-Ping et al., 1992; Li et al., 2014; McCutchen-Maloney et al., 2000; Yashiroda et al., 2015; Zaiss et al., 1999). In support of this idea, PI31 promoted the formation of proteasome-DYNLL1/2 complexes in cells and *in vitro*, and inactivation of PI31 disrupted axonal proteasome movement and caused functional and structural defects of *Drosophila* neurons. In particular, elimination of PI31 in neurons caused defects in synaptic morphology, and mosaic analysis demonstrated that this reflects a cell-autonomous requirement for PI31 in neurons. Furthermore, loss of PI31 function led to the accumulation of Poly-Ub aggregates at nerve terminals and in axons, consistent with the idea that insufficient amounts of proteasomes were available in the periphery of neurons for proper protein degradation. Collectively, our results suggest that PI31 is a direct adaptor for microtubule-dependent transport of proteasomes and thereby promotes allocation of proteasomes to synapses (Figure 9).

This study also revealed a role of p38 MAPK-mediated phosphorylation of PI31 in the formation of proteasome-DYNLL1/2 complexes. Phosphorylation of a conserved site in both *Drosophila* and human PI31 promoted binding to DYNLL1/2 and stimulated the formation of proteasome-DYNLL1/2 complexes. Importantly, mutating the phospho-acceptor site of PI31 (*PI31*^{S168A} *knock-in*) impaired proteasome transport in axons. This suggests that PI31 phosphorylation serves as a molecular switch to regulate proteasome movement (Figure 9). Since phosphorylation is a dynamic and labile post-translational modification, PI31 may use phosphorylation to receive various internal and external signals through kinases and phosphatase activity. p38 MAPKs can be activated by a wide range of cellular stresses, including proteotoxic stress (Cuenda and Rousseau, 2007; Zarubin and Han, 2005). Our findings are consistent with the idea that p38 MAPKs stimulates proteasome movement in response to stress by promoting the formation of proteasome-DYNLL1/2 complexes.

This study may help reconcile somewhat conflicting reports in the literature. PI31 was initially identified as a proteasome-interacting protein, and binding of PI31 to 20S particles can inhibit peptide proteolysis *in vitro*(Bader et al., 2011; Chu-Ping et al., 1992; McCutchen-Maloney et al., 2000; Zaiss et al., 1999). On the other hand, genetic studies in both yeast and *Drosophila* indicate that the physiological function of PI31 is to promote protein breakdown(Bader et al., 2011; Yashiroda et al., 2015). It is also worth noting that PI31 activity is subject to post-translational modification, and that large cells, such as spermatids and neurons are particular sensitive to the loss of PI31 (Bader et al., 2011; Cho-Park and Steller, 2013). In contrast, no overt requirements for PI31 were detected in cultured HEK293 cells, and PI31-inactivation produces only modest biochemical changes at the level of whole-cell extracts(Cho-Park and Steller, 2013; Li et al., 2014). The mechanism reported here provides an explanation for these seemingly conflicting reports as it reveals a role of PI31 for localized regulation of proteasomes. Such a localized function is not readily detectable by standard methodologies for assessing proteasome activity in whole-cell extracts.

The results presented here may also have important implications for human neurological disorders. Many age-related neurodegenerative diseases, including Alzheimer's Disease (AD) and Parkinson's Disease (PD), are characterized by the accumulation of protein aggregates(Ballatore et al., 2007; Irvine et al., 2008; Li and Li, 2011; Oddo, 2008; Ross and Poirier, 2004; Tai and Schuman, 2008). The proteins in these pathognomonic aggregates are typically ubiquitin-conjugated (Bilen and Bonini, 2005; de Vrij et al., 2004; Mori et al., 1987; Morimoto, 2008; Morishima-Kawashima et al., 1993; Perry et al., 1987; Rubinsztein, 2006; Zoghbi and Orr, 2000). This suggests that the affected neurons attempted to remove abnormal proteins by tagging them with ubiquitin, but subsequently failed to degrade them. One possible explanation for this is that proteasomes were not available in sufficient numbers to degrade all ubiquitin-conjugates. Because the first signs of impaired proteostasis and accumulation of pathological proteins are generally seen in the periphery of neurons, it has been suggested that defects in proteasome transport may be responsible for abnormal protein clearance in neurodegenerative diseases(Coleman and Perry, 2002; Gendron and Petrucelli, 2009;

Hoover et al., 2010; Ittner et al., 2010; Otero et al., 2014; Yoshiyama et al., 2007; Yu and Lu, 2012). PI31 is implicated in this process since human mutations affecting PI31 activity are associated with neurodegenerative diseases, including AD, PD and amyotrophic lateral sclerosis (ALS)(Aguado et al., 2010; Conedera et al., 2016; Di Fonzo et al., 2009; Johnson et al., 2010; Koppers et al., 2012; Paisan-Ruiz et al., 2010; Sherva et al., 2011). Perhaps the most compelling case for linking PI31 with human disease comes from the analysis of *FBXO7/PARK15* mutants. Mutations in this gene lead to an early, familiar form of PD in humans, and inactivation of FBXO7 in mice causes neuronal degeneration and PD-like phenotypes (Conedera et al., 2016; Di Fonzo et al., 2009; Paisan-Ruiz et al., 2010; Vingill et al., 2016). FBXO7 is a strong and direct binding partner of PI31 in both insects and mammals, and loss of FBXO7 function results in proteolytic cleavage and reduced levels of PI31(Bader et al., 2011; Kirk et al., 2008). Strikingly, *FBXO7*-null mice were found to have significantly reduced PI31 levels, but a critical function of PI31 was dismissed based on analysis of whole-cell extracts(Vingill et al., 2016). Since a role of PI31 in proteasome transport would not have been detected by this approach, we suggest that this topic deserves further investigation. Finally, p38 MAPKs are involved in synaptic plasticity, learning and memory(Giese and Mizuno, 2013). These kinases have also been implicated in the pathogenesis of various human neurological diseases, including AD, PD, ALS, ischemia, neuropathic pain, epilepsy and depression (Cuenda and Rousseau, 2007; Jha et al., 2015; Kim and Choi, 2010; Lee and Kim, 2017; Munoz and Ammit, 2010; Yasuda et al., 2011). Our results link p38 MAPKs with the regulation of proteasome transport and raise the intriguing possibility that mis-regulation of proteasome transport contributes to the pathogenesis of p38 MAPK-associated neurological disorders.

Acknowledgement

We thank Dr. Aaron DiAntonio for the GluRIIC antibody; Dr. Benjamin Eaton, the Bloomington *Drosophila* Stock Center, Vienna *Drosophila* Resource Center, FlyLight project team of Janelia Research Campus, and Flybase for *Drosophila* strains and relevant information. We are also grateful to Drs. Park Cho-Park, Simon Bullock, Michael Davidson, Didier Trono and Steven Vogel, and Addgene for plasmids. We thank Yetis Gultekin for his help in constructing the pLVX-EF1a-AcGFP-C1-mPI31 plasmid and generation of anti-PI31 antibody, and Drs. Alison North and Christina Pyrgaki for their help with live-imaging analysis. We also thank Drs. Michael Young, Brian Chait, Sarit Larisch, Park Cho-Park, Xiaochun Li, Mia Horowitz, Avi Levin, Sigi Benjamin-Hong, Dolors Ferres-Marco, Thomas Hsiao, Junko Shimazu, Wanhe Li, Erica Jacobs, Junjie Wang, and Alana Persaud for valuable discussions. This work was supported by NIH grant RO1GM60124 and a generous gift from the Loewenberg Foundation to H.S.

Author Contributions

Conceptualization, K.L. and H.S.; Investigation, K.L., S.J., A.M., J.R., and H.M.; Resources, H.S.; Writing, K.L. and H.S.; Funding Acquisition, H.S.; Supervision, H.S.

Declaration of Interests

The authors declare no competing interests.

References

Aguado, C., Sarkar, S., Korolchuk, V.I., Criado, O., Vernia, S., Boya, P., Sanz, P., de Cordoba, S.R., Knecht, E., and Rubinsztein, D.C. (2010). Laforin, the most common protein mutated in Lafora disease, regulates autophagy. Human molecular genetics *19*, 2867-2876.

Asano, S., Fukuda, Y., Beck, F., Aufderheide, A., Forster, F., Danev, R., and Baumeister, W. (2015). Proteasomes. A molecular census of 26S proteasomes in intact neurons. Science *347*, 439-442.

Bader, M., Benjamin, S., Wapinski, O.L., Smith, D.M., Goldberg, A.L., and Steller, H. (2011). A conserved F box regulatory complex controls proteasome activity in Drosophila. Cell *145*, 371-382.

Bai, C., Sen, P., Hofmann, K., Ma, L., Goebl, M., Harper, J.W., and Elledge, S.J. (1996). SKP1 connects cell cycle regulators to the ubiquitin proteolysis machinery through a novel motif, the F-box. Cell *86*, 263-274.

Balch, W.E., Morimoto, R.I., Dillin, A., and Kelly, J.W. (2008). Adapting proteostasis for disease intervention. Science *319*, 916-919.

Ballatore, C., Lee, V.M., and Trojanowski, J.Q. (2007). Tau-mediated neurodegeneration in Alzheimer's disease and related disorders. Nat Rev Neurosci *8*, 663-672.

Baumeister, W., Walz, J., Zuhl, F., and Seemuller, E. (1998). The proteasome: paradigm of a self-compartmentalizing protease. Cell *92*, 367-380.

Bento, C.F., Renna, M., Ghislat, G., Puri, C., Ashkenazi, A., Vicinanza, M., Menzies, F.M., and Rubinsztein, D.C. (2016). Mammalian Autophagy: How Does It Work? Annual review of biochemistry *85*, 685-713.

Bilen, J., and Bonini, N.M. (2005). Drosophila as a model for human neurodegenerative disease. Annual review of genetics *39*, 153-171.

Bingol, B., and Schuman, E.M. (2006). Activity-dependent dynamics and sequestration of proteasomes in dendritic spines. Nature *441*, 1144-1148.

Bingol, B., and Sheng, M. (2011). Deconstruction for reconstruction: the role of proteolysis in neural plasticity and disease. Neuron *69*, 22-32.

Bingol, B., Wang, C.F., Arnott, D., Cheng, D., Peng, J., and Sheng, M. (2010). Autophosphorylated CaMKIIalpha acts as a scaffold to recruit proteasomes to dendritic spines. Cell *140*, 567-578.

Bischof, J., Maeda, R.K., Hediger, M., Karch, F., and Basler, K. (2007). An optimized transgenesis system for Drosophila using germ-line-specific phiC31 integrases. Proceedings of the National Academy of Sciences of the United States of America *104*, 3312-3317.

Campbell, D.S., and Holt, C.E. (2001). Chemotropic responses of retinal growth cones mediated by rapid local protein synthesis and degradation. Neuron *32*, 1013-1026.

Chintapalli, V.R., Wang, J., and Dow, J.A. (2007). Using FlyAtlas to identify better Drosophila melanogaster models of human disease. Nature genetics *39*, 715-720.

Cho-Park, P.F., and Steller, H. (2013). Proteasome regulation by ADP-ribosylation. Cell *153*, 614-627.

Chu-Ping, M., Slaughter, C.A., and DeMartino, G.N. (1992). Purification and characterization of a protein inhibitor of the 20S proteasome (macropain). Biochimica et biophysica acta *1119*, 303-311.
Clemen, C.S., Marko, M., Strucksberg, K.H., Behrens, J., Wittig, I., Gartner, L., Winter, L., Chevessier, F., Matthias, J., Turk, M.*, et al.* (2015). VCP and PSMF1: Antagonistic regulators of proteasome activity. Biochemical and biophysical research communications *463*, 1210-1217.
Coleman, M.P., and Perry, V.H. (2002). Axon pathology in neurological disease: a neglected therapeutic target. Trends in neurosciences *25*, 532-537.
Collins, G.A., and Goldberg, A.L. (2017). The Logic of the 26S Proteasome. Cell *169*, 792-806.
Conedera, S., Apaydin, H., Li, Y., Yoshino, H., Ikeda, A., Matsushima, T., Funayama, M., Nishioka, K., and Hattori, N. (2016). FBXO7 mutations in Parkinson's disease and multiple system atrophy. Neurobiology of aging *40*, 192 e191-192 e195.
Cox, J., Hein, M.Y., Luber, C.A., Paron, I., Nagaraj, N., and Mann, M. (2014). Accurate proteome-wide label-free quantification by delayed normalization and maximal peptide ratio extraction, termed MaxLFQ. Molecular & cellular proteomics : MCP *13*, 2513-2526.
Cuenda, A., and Rousseau, S. (2007). p38 MAP-kinases pathway regulation, function and role in human diseases. Biochimica et biophysica acta *1773*, 1358-1375.
de Vrij, F.M., Fischer, D.F., van Leeuwen, F.W., and Hol, E.M. (2004). Protein quality control in Alzheimer's disease by the ubiquitin proteasome system. Prog Neurobiol *74*, 249-270.
Di Fonzo, A., Dekker, M.C., Montagna, P., Baruzzi, A., Yonova, E.H., Correia Guedes, L., Szczerbinska, A., Zhao, T., Dubbel-Hulsman, L.O., Wouters, C.H.*, et al.* (2009). FBXO7 mutations cause autosomal recessive, early-onset parkinsonian-pyramidal syndrome. Neurology *72*, 240-245.
DiAntonio, A., Haghighi, A.P., Portman, S.L., Lee, J.D., Amaranto, A.M., and Goodman, C.S. (2001). Ubiquitination-dependent mechanisms regulate synaptic growth and function. Nature *412*, 449-452.
Dikic, I., and Elazar, Z. (2018). Mechanism and medical implications of mammalian autophagy. Nature reviews Molecular cell biology *19*, 349-364.
Ding, M., Chao, D., Wang, G., and Shen, K. (2007). Spatial regulation of an E3 ubiquitin ligase directs selective synapse elimination. Science *317*, 947-951.
Djakovic, S.N., Marquez-Lona, E.M., Jakawich, S.K., Wright, R., Chu, C., Sutton, M.A., and Patrick, G.N. (2012). Phosphorylation of Rpt6 regulates synaptic strength in hippocampal neurons. The Journal of neuroscience : the official journal of the Society for Neuroscience *32*, 5126-5131.
Djakovic, S.N., Schwarz, L.A., Barylko, B., DeMartino, G.N., and Patrick, G.N. (2009). Regulation of the proteasome by neuronal activity and calcium/calmodulin-dependent protein kinase II. The Journal of biological chemistry *284*, 26655-26665.
Ehlers, M.D. (2003). Activity level controls postsynaptic composition and signaling via the ubiquitin-proteasome system. Nature neuroscience *6*, 231-242.
Erturk, A., Wang, Y., and Sheng, M. (2014). Local pruning of dendrites and spines by caspase-3-dependent and proteasome-limited mechanisms. The Journal of neuroscience : the official journal of the Society for Neuroscience *34*, 1672-1688.

Gendron, T.F., and Petrucelli, L. (2009). The role of tau in neurodegeneration. Molecular neurodegeneration *4*, 13.
Giese, K.P., and Mizuno, K. (2013). The roles of protein kinases in learning and memory. Learning & memory *20*, 540-552.
Glickman, M.H., and Ciechanover, A. (2002). The ubiquitin-proteasome proteolytic pathway: destruction for the sake of construction. Physiological reviews *82*, 373-428.
Goldberg, A.L. (2003). Protein degradation and protection against misfolded or damaged proteins. Nature *426*, 895-899.
Gratz, S.J., Ukken, F.P., Rubinstein, C.D., Thiede, G., Donohue, L.K., Cummings, A.M., and O'Connor-Giles, K.M. (2014). Highly specific and efficient CRISPR/Cas9-catalyzed homology-directed repair in Drosophila. Genetics *196*, 961-971.
Hamilton, A.M., and Zito, K. (2013). Breaking it down: the ubiquitin proteasome system in neuronal morphogenesis. Neural Plast *2013*, 196848.
Han, J., Lee, J.D., Bibbs, L., and Ulevitch, R.J. (1994). A MAP kinase targeted by endotoxin and hyperosmolarity in mammalian cells. Science *265*, 808-811.
Hegde, A.N., Haynes, K.A., Bach, S.V., and Beckelman, B.C. (2014). Local ubiquitin-proteasome-mediated proteolysis and long-term synaptic plasticity. Frontiers in molecular neuroscience *7*, 96.
Heigwer, F., Kerr, G., and Boutros, M. (2014). E-CRISP: fast CRISPR target site identification. Nature methods *11*, 122-123.
Hirokawa, N., Niwa, S., and Tanaka, Y. (2010). Molecular motors in neurons: transport mechanisms and roles in brain function, development, and disease. Neuron *68*, 610-638.
Hoover, B.R., Reed, M.N., Su, J., Penrod, R.D., Kotilinek, L.A., Grant, M.K., Pitstick, R., Carlson, G.A., Lanier, L.M., Yuan, L.L.*, et al.* (2010). Tau mislocalization to dendritic spines mediates synaptic dysfunction independently of neurodegeneration. Neuron *68*, 1067-1081.
Hsu, M.T., Guo, C.L., Liou, A.Y., Chang, T.Y., Ng, M.C., Florea, B.I., Overkleeft, H.S., Wu, Y.L., Liao, J.C., and Cheng, P.L. (2015). Stage-Dependent Axon Transport of Proteasomes Contributes to Axon Development. Developmental cell *35*, 418-431.
Irvine, G.B., El-Agnaf, O.M., Shankar, G.M., and Walsh, D.M. (2008). Protein aggregation in the brain: the molecular basis for Alzheimer's and Parkinson's diseases. Mol Med *14*, 451-464.
Ittner, L.M., Ke, Y.D., Delerue, F., Bi, M., Gladbach, A., van Eersel, J., Wolfing, H., Chieng, B.C., Christie, M.J., Napier, I.A.*, et al.* (2010). Dendritic function of tau mediates amyloid-beta toxicity in Alzheimer's disease mouse models. Cell *142*, 387-397.
Jan, L.Y., and Jan, Y.N. (1982). Antibodies to horseradish peroxidase as specific neuronal markers in Drosophila and in grasshopper embryos. Proceedings of the National Academy of Sciences of the United States of America *79*, 2700-2704.
Jha, S.K., Jha, N.K., Kar, R., Ambasta, R.K., and Kumar, P. (2015). p38 MAPK and PI3K/AKT Signalling Cascades inParkinson's Disease. International journal of molecular and cellular medicine *4*, 67-86.

Johnson, J.O., Mandrioli, J., Benatar, M., Abramzon, Y., Van Deerlin, V.M., Trojanowski, J.Q., Gibbs, J.R., Brunetti, M., Gronka, S., Wuu, J.*, et al.* (2010). Exome sequencing reveals VCP mutations as a cause of familial ALS. Neuron *68*, 857-864.
Kall, L., Canterbury, J.D., Weston, J., Noble, W.S., and MacCoss, M.J. (2007). Semi-supervised learning for peptide identification from shotgun proteomics datasets. Nature methods *4*, 923-925.
Kim, E.K., and Choi, E.J. (2010). Pathological roles of MAPK signaling pathways in human diseases. Biochimica et biophysica acta *1802*, 396-405.
Kipreos, E.T., and Pagano, M. (2000). The F-box protein family. Genome biology *1*, REVIEWS3002.
Kirk, R., Laman, H., Knowles, P.P., Murray-Rust, J., Lomonosov, M., Meziane el, K., and McDonald, N.Q. (2008). Structure of a conserved dimerization domain within the F-box protein Fbxo7 and the PI31 proteasome inhibitor. The Journal of biological chemistry *283*, 22325-22335.
Kittel, R.J., Wichmann, C., Rasse, T.M., Fouquet, W., Schmidt, M., Schmid, A., Wagh, D.A., Pawlu, C., Kellner, R.R., Willig, K.I.*, et al.* (2006). Bruchpilot promotes active zone assembly, Ca2+ channel clustering, and vesicle release. Science *312*, 1051-1054.
Koppers, M., van Blitterswijk, M.M., Vlam, L., Rowicka, P.A., van Vught, P.W., Groen, E.J., Spliet, W.G., Engelen-Lee, J., Schelhaas, H.J., de Visser, M.*, et al.* (2012). VCP mutations in familial and sporadic amyotrophic lateral sclerosis. Neurobiology of aging *33*, 837 e837-813.
Koushik, S.V., Chen, H., Thaler, C., Puhl, H.L., 3rd, and Vogel, S.S. (2006). Cerulean, Venus, and VenusY67C FRET reference standards. Biophysical journal *91*, L99-L101.
Kreko-Pierce, T., and Eaton, B.A. (2017). The Drosophila LC8 homolog cut up specifies the axonal transport of proteasomes. Journal of cell science *130*, 3388-3398.
Kuo, C.T., Jan, L.Y., and Jan, Y.N. (2005). Dendrite-specific remodeling of Drosophila sensory neurons requires matrix metalloproteases, ubiquitin-proteasome, and ecdysone signaling. Proceedings of the National Academy of Sciences of the United States of America *102*, 15230-15235.
Labbadia, J., and Morimoto, R.I. (2015). The biology of proteostasis in aging and disease. Annual review of biochemistry *84*, 435-464.
Lecker, S.H., Solomon, V., Mitch, W.E., and Goldberg, A.L. (1999). Muscle protein breakdown and the critical role of the ubiquitin-proteasome pathway in normal and disease states. The Journal of nutrition *129*, 227S-237S.
Lee, J.K., and Kim, N.J. (2017). Recent Advances in the Inhibition of p38 MAPK as a Potential Strategy for the Treatment of Alzheimer's Disease. Molecules *22*.
Lee, S.H., Choi, J.H., Lee, N., Lee, H.R., Kim, J.I., Yu, N.K., Choi, S.L., Lee, S.H., Kim, H., and Kaang, B.K. (2008). Synaptic protein degradation underlies destabilization of retrieved fear memory. Science *319*, 1253-1256.
Levine, B., and Kroemer, G. (2008). Autophagy in the pathogenesis of disease. Cell *132*, 27-42.
Li, X., Thompson, D., Kumar, B., and DeMartino, G.N. (2014). Molecular and cellular roles of PI31 (PSMF1) protein in regulation of proteasome function. The Journal of biological chemistry *289*, 17392-17405.

Li, X.J., and Li, S. (2011). Proteasomal dysfunction in aging and Huntington disease. Neurobiology of disease *43*, 4-8.
Liu, C.W., Li, X., Thompson, D., Wooding, K., Chang, T.L., Tang, Z., Yu, H., Thomas, P.J., and DeMartino, G.N. (2006). ATP binding and ATP hydrolysis play distinct roles in the function of 26S proteasome. Molecular cell *24*, 39-50.
Marrus, S.B., Portman, S.L., Allen, M.J., Moffat, K.G., and DiAntonio, A. (2004). Differential localization of glutamate receptor subunits at the Drosophila neuromuscular junction. The Journal of neuroscience : the official journal of the Society for Neuroscience *24*, 1406-1415.
McCutchen-Maloney, S.L., Matsuda, K., Shimbara, N., Binns, D.D., Tanaka, K., Slaughter, C.A., and DeMartino, G.N. (2000). cDNA cloning, expression, and functional characterization of PI31, a proline-rich inhibitor of the proteasome. The Journal of biological chemistry *275*, 18557-18565.
Mori, H., Kondo, J., and Ihara, Y. (1987). Ubiquitin is a component of paired helical filaments in Alzheimer's disease. Science *235*, 1641-1644.
Morimoto, R.I. (2008). Proteotoxic stress and inducible chaperone networks in neurodegenerative disease and aging. Genes & development *22*, 1427-1438.
Morishima-Kawashima, M., Hasegawa, M., Takio, K., Suzuki, M., Titani, K., and Ihara, Y. (1993). Ubiquitin is conjugated with amino-terminally processed tau in paired helical filaments. Neuron *10*, 1151-1160.
Munoz, L., and Ammit, A.J. (2010). Targeting p38 MAPK pathway for the treatment of Alzheimer's disease. Neuropharmacology *58*, 561-568.
Murata, S., Yashiroda, H., and Tanaka, K. (2009). Molecular mechanisms of proteasome assembly. Nature reviews Molecular cell biology *10*, 104-115.
Nakatogawa, H., Suzuki, K., Kamada, Y., and Ohsumi, Y. (2009). Dynamics and diversity in autophagy mechanisms: lessons from yeast. Nature reviews Molecular cell biology *10*, 458-467.
Ni, J.Q., Markstein, M., Binari, R., Pfeiffer, B., Liu, L.P., Villalta, C., Booker, M., Perkins, L., and Perrimon, N. (2008). Vector and parameters for targeted transgenic RNA interference in Drosophila melanogaster. Nature methods *5*, 49-51.
Oddo, S. (2008). The ubiquitin-proteasome system in Alzheimer's disease. J Cell Mol Med *12*, 363-373.
Olenych, S.G., Claxton, N.S., Ottenberg, G.K., and Davidson, M.W. (2007). The fluorescent protein color palette. Current protocols in cell biology *Chapter 21*, Unit 21 25.
Otero, M.G., Alloatti, M., Cromberg, L.E., Almenar-Queralt, A., Encalada, S.E., Pozo Devoto, V.M., Bruno, L., Goldstein, L.S., and Falzone, T.L. (2014). Fast axonal transport of the proteasome complex depends on membrane interaction and molecular motor function. Journal of cell science *127*, 1537-1549.
Paisan-Ruiz, C., Guevara, R., Federoff, M., Hanagasi, H., Sina, F., Elahi, E., Schneider, S.A., Schwingenschuh, P., Bajaj, N., Emre, M.*, et al.* (2010). Early-onset L-dopa-responsive parkinsonism with pyramidal signs due to ATP13A2, PLA2G6, FBXO7 and spatacsin mutations. Movement disorders : official journal of the Movement Disorder Society *25*, 1791-1800.
Pak, D.T., and Sheng, M. (2003). Targeted protein degradation and synapse remodeling by an inducible protein kinase. Science *302*, 1368-1373.

Patrick, G.N. (2006). Synapse formation and plasticity: recent insights from the perspective of the ubiquitin proteasome system. Current opinion in neurobiology *16*, 90-94.
Perry, G., Friedman, R., Shaw, G., and Chau, V. (1987). Ubiquitin is detected in neurofibrillary tangles and senile plaque neurites of Alzheimer disease brains. Proceedings of the National Academy of Sciences of the United States of America *84*, 3033-3036.
Pfeiffer, B.D., Jenett, A., Hammonds, A.S., Ngo, T.T., Misra, S., Murphy, C., Scully, A., Carlson, J.W., Wan, K.H., Laverty, T.R*., et al.* (2008). Tools for neuroanatomy and neurogenetics in Drosophila. Proceedings of the National Academy of Sciences of the United States of America *105*, 9715-9720.
Pfeiffer, B.D., Ngo, T.T., Hibbard, K.L., Murphy, C., Jenett, A., Truman, J.W., and Rubin, G.M. (2010). Refinement of tools for targeted gene expression in Drosophila. Genetics *186*, 735-755.
Port, F., Chen, H.M., Lee, T., and Bullock, S.L. (2014). Optimized CRISPR/Cas tools for efficient germline and somatic genome engineering in Drosophila. Proceedings of the National Academy of Sciences of the United States of America *111*, E2967-2976.
Qian, M.X., Pang, Y., Liu, C.H., Haratake, K., Du, B.Y., Ji, D.Y., Wang, G.F., Zhu, Q.Q., Song, W., Yu, Y*., et al.* (2013). Acetylation-mediated proteasomal degradation of core histones during DNA repair and spermatogenesis. Cell *153*, 1012-1024.
Ramachandran, K.V., Fu, J.M., Schaffer, T.B., Na, C.H., Delannoy, M., and Margolis, S.S. (2018). Activity-Dependent Degradation of the Nascentome by the Neuronal Membrane Proteasome. Molecular cell *71*, 169-177 e166.
Ramachandran, K.V., and Margolis, S.S. (2017). A mammalian nervous-system-specific plasma membrane proteasome complex that modulates neuronal function. Nature structural & molecular biology *24*, 419-430.
Rappsilber, J., Mann, M., and Ishihama, Y. (2007). Protocol for micro-purification, enrichment, pre-fractionation and storage of peptides for proteomics using StageTips. Nature protocols *2*, 1896-1906.
Reck-Peterson, S.L., Redwine, W.B., Vale, R.D., and Carter, A.P. (2018). The cytoplasmic dynein transport machinery and its many cargoes. Nature reviews Molecular cell biology *19*, 382-398.
Ren, X., Sun, J., Housden, B.E., Hu, Y., Roesel, C., Lin, S., Liu, L.P., Yang, Z., Mao, D., Sun, L*., et al.* (2013). Optimized gene editing technology for Drosophila melanogaster using germ line-specific Cas9. Proceedings of the National Academy of Sciences of the United States of America *110*, 19012-19017.
Ross, C.A., and Poirier, M.A. (2004). Protein aggregation and neurodegenerative disease. Nature medicine *10 Suppl*, S10-17.
Rubinsztein, D.C. (2006). The roles of intracellular protein-degradation pathways in neurodegeneration. Nature *443*, 780-786.
Sandri, M. (2013). Protein breakdown in muscle wasting: role of autophagy-lysosome and ubiquitin-proteasome. The international journal of biochemistry & cell biology *45*, 2121-2129.
Sanyal, S. (2009). Genomic mapping and expression patterns of C380, OK6 and D42 enhancer trap lines in the larval nervous system of Drosophila. Gene expression patterns : GEP *9*, 371-380.

Schindelin, J., Arganda-Carreras, I., Frise, E., Kaynig, V., Longair, M., Pietzsch, T., Preibisch, S., Rueden, C., Saalfeld, S., Schmid, B.*, et al.* (2012). Fiji: an open-source platform for biological-image analysis. Nature methods *9*, 676-682.
Schliwa, M., and Woehlke, G. (2003). Molecular motors. Nature *422*, 759-765.
Schmidt, M., and Finley, D. (2014). Regulation of proteasome activity in health and disease. Biochimica et biophysica acta *1843*, 13-25.
Schwanhausser, B., Busse, D., Li, N., Dittmar, G., Schuchhardt, J., Wolf, J., Chen, W., and Selbach, M. (2011). Global quantification of mammalian gene expression control. Nature *473*, 337-342.
Sherva, R., Baldwin, C.T., Inzelberg, R., Vardarajan, B., Cupples, L.A., Lunetta, K., Bowirrat, A., Naj, A., Pericak-Vance, M., Friedland, R.P.*, et al.* (2011). Identification of novel candidate genes for Alzheimer's disease by autozygosity mapping using genome wide SNP data. Journal of Alzheimer's disease : JAD *23*, 349-359.
Sigrist, S.J. (2009). The Yin and Yang of synaptic active zone assembly. Science signaling *2*, pe32.
Skaar, J.R., Pagan, J.K., and Pagano, M. (2013). Mechanisms and function of substrate recruitment by F-box proteins. Nat Rev Mol Cell Biol *14*, 369-381.
Skowyra, D., Craig, K.L., Tyers, M., Elledge, S.J., and Harper, J.W. (1997). F-box proteins are receptors that recruit phosphorylated substrates to the SCF ubiquitin-ligase complex. Cell *91*, 209-219.
Speese, S.D., Trotta, N., Rodesch, C.K., Aravamudan, B., and Broadie, K. (2003). The ubiquitin proteasome system acutely regulates presynaptic protein turnover and synaptic efficacy. Current biology : CB *13*, 899-910.
Sun, B., Xu, P., and Salvaterra, P.M. (1999). Dynamic visualization of nervous system in live Drosophila. Proceedings of the National Academy of Sciences of the United States of America *96*, 10438-10443.
Tai, H.C., and Schuman, E.M. (2008). Ubiquitin, the proteasome and protein degradation in neuronal function and dysfunction. Nature reviews Neuroscience *9*, 826-838.
Tyanova, S., Temu, T., Sinitcyn, P., Carlson, A., Hein, M.Y., Geiger, T., Mann, M., and Cox, J. (2016). The Perseus computational platform for comprehensive analysis of (prote)omics data. Nature methods *13*, 731-740.
Valakh, V., Naylor, S.A., Berns, D.S., and DiAntonio, A. (2012). A large-scale RNAi screen identifies functional classes of genes shaping synaptic development and maintenance. Developmental biology *366*, 163-171.
Vale, R.D. (2003). The molecular motor toolbox for intracellular transport. Cell *112*, 467-480.
Varshavsky, A. (2005). Regulated protein degradation. Trends in biochemical sciences *30*, 283-286.
Vilchez, D., Saez, I., and Dillin, A. (2014). The role of protein clearance mechanisms in organismal ageing and age-related diseases. Nature communications *5*, 5659.
Vingill, S., Brockelt, D., Lancelin, C., Tatenhorst, L., Dontcheva, G., Preisinger, C., Schwedhelm-Domeyer, N., Joseph, S., Mitkovski, M., Goebbels, S.*, et al.* (2016). Loss of FBXO7 (PARK15) results in reduced proteasome activity and models a parkinsonism-like phenotype in mice. The EMBO journal *35*, 2008-2025.

Wagh, D.A., Rasse, T.M., Asan, E., Hofbauer, A., Schwenkert, I., Durrbeck, H., Buchner, S., Dabauvalle, M.C., Schmidt, M., Qin, G.*, et al.* (2006). Bruchpilot, a protein with homology to ELKS/CAST, is required for structural integrity and function of synaptic active zones in Drosophila. Neuron *49*, 833-844.
Wagih, O., Sugiyama, N., Ishihama, Y., and Beltrao, P. (2016). Uncovering Phosphorylation-Based Specificities through Functional Interaction Networks. Molecular & cellular proteomics : MCP *15*, 236-245.
Wan, H.I., DiAntonio, A., Fetter, R.D., Bergstrom, K., Strauss, R., and Goodman, C.S. (2000). Highwire regulates synaptic growth in Drosophila. Neuron *26*, 313-329.
Watts, R.J., Hoopfer, E.D., and Luo, L. (2003). Axon pruning during Drosophila metamorphosis: evidence for local degeneration and requirement of the ubiquitin-proteasome system. Neuron *38*, 871-885.
Willeumier, K., Pulst, S.M., and Schweizer, F.E. (2006). Proteasome inhibition triggers activity-dependent increase in the size of the recycling vesicle pool in cultured hippocampal neurons. The Journal of neuroscience : the official journal of the Society for Neuroscience *26*, 11333-11341.
Wolff, S., Weissman, J.S., and Dillin, A. (2014). Differential scales of protein quality control. Cell *157*, 52-64.
Wu, J.S., and Luo, L. (2006). A protocol for mosaic analysis with a repressible cell marker (MARCM) in Drosophila. Nature protocols *1*, 2583-2589.
Yashiroda, H., Toda, Y., Otsu, S., Takagi, K., Mizushima, T., and Murata, S. (2015). N-terminal alpha7 deletion of the proteasome 20S core particle substitutes for yeast PI31 function. Molecular and cellular biology *35*, 141-152.
Yasuda, S., Sugiura, H., Tanaka, H., Takigami, S., and Yamagata, K. (2011). p38 MAP kinase inhibitors as potential therapeutic drugs for neural diseases. Central nervous system agents in medicinal chemistry *11*, 45-59.
Yi, J.J., and Ehlers, M.D. (2005). Ubiquitin and protein turnover in synapse function. Neuron *47*, 629-632.
Yoshiyama, Y., Higuchi, M., Zhang, B., Huang, S.M., Iwata, N., Saido, T.C., Maeda, J., Suhara, T., Trojanowski, J.Q., and Lee, V.M. (2007). Synapse loss and microglial activation precede tangles in a P301S tauopathy mouse model. Neuron *53*, 337-351.
Yu, W., and Lu, B. (2012). Synapses and dendritic spines as pathogenic targets in Alzheimer's disease. Neural Plast *2012*, 247150.
Zaiss, D.M., Standera, S., Holzhutter, H., Kloetzel, P., and Sijts, A.J. (1999). The proteasome inhibitor PI31 competes with PA28 for binding to 20S proteasomes. FEBS letters *457*, 333-338.
Zarubin, T., and Han, J. (2005). Activation and signaling of the p38 MAP kinase pathway. Cell research *15*, 11-18.
Zhao, Y., Hegde, A.N., and Martin, K.C. (2003). The ubiquitin proteasome system functions as an inhibitory constraint on synaptic strengthening. Current biology : CB *13*, 887-898.
Zhong, L., and Belote, J.M. (2007). The testis-specific proteasome subunit Prosalpha6T of D. melanogaster is required for individualization and nuclear maturation during spermatogenesis. Development *134*, 3517-3525.
Zhu, G., Fujii, K., Belkina, N., Liu, Y., James, M., Herrero, J., and Shaw, S. (2005). Exceptional disfavor for proline at the P + 1 position among AGC and CAMK kinases

establishes reciprocal specificity between them and the proline-directed kinases. The Journal of biological chemistry *280*, 10743-10748.
Zoghbi, H.Y., and Orr, H.T. (2000). Glutamine repeats and neurodegeneration. Annual review of neuroscience *23*, 217-247.

Figure Legends

Figure 1. PI31 is required for proteostasis and synaptic structure and function in motor neurons.

(**A**) PI31 forms puncta in axons and at neuromuscular junctions (NMJs) of *Drosophila* motor neurons. The expression of *UAS-HA-PI31* was driven by *R94G06-GAL4*, a specific motor neuron driver (see Figure S1A). HA antibody (green) labels HA-PI31, and HRP antibody (red) marks neuronal membranes.

(**B and C**) Representative images (**B**) and quantification(**C**) showing that loss of PI31 leads to accumulation of poly-ubiquitinated (Poly-Ub) protein puncta in axons of *Drosophila* motor neurons. Poly-Ub proteins were stained with a widely used Ub-conjugates antibody (clone FK2, green), and HRP antibody (red) labeled neuronal membranes to visualize axons. Poly-Ub protein puncta from three different microscope views were counted for each larva. The numbers were added together and normalized by the total area of axons. n=5 larvae for each genotype. Mean+s.e.m., unpaired two-tailed t-test, * $P<0.05$.

(**D and E**) Representative images (**D**) and quantification (**E**) showing that loss of PI31 leads to accumulation of Poly-Ub proteins at NMJs of *Drosophila* motor neurons. Immuofluorecence intensities of Poly-Ub proteins were measured and normalized for the NMJ area. n=20 M4 NMJs from four larvae for each genotype. Mean+s.e.m. Unpaired two-tailed t-test, *** $P<0.001$.

(**F and G**) High-magnification images (**F**) and quantification (**G**) of Brp puncta at NMJs indicate that loss of PI31 leads to the reduction of the core active zone (AZ) scaffold protein Brp puncta at NMJs, suggesting a structural defect of synapses in *PI31*$^{-/-}$ larvae. n=20 NMJs from four larvae for M4, and n=10 NMJs from six larvae for M6/7 at A2 segments. Mean+s.e.m., unpaired two-tailed t-test, *** $P<0.001$. The overview of M4 NMJs is shown in Figure S1B, and see Figure S1C and D for the overview and high-magnification images of M6/7 NMJs.

(**H**) Frequency distribution plot of Brp punctum volumes of M4 NMJs demonstrates that small Brp puncta (volume<0.5μm^3) are specifically affected by loss of PI31. n=6853 Brp puncta from 20 NMJs for wild-type, and n= 3672 Brp puncta from 20 NMJs for *PI31*$^{-/-}$.

(**I and J**) Representative images (**I**) and quantification (**J**) of MARCM experiments show that the loss of Brp puncta at *PI31*$^{-/-}$ NMJs is a neuron-autonomous phenotype. GFP^{+} is *PI31*$^{-/-}$, and GFP^{-} is *PI31*$^{+/-}$ from the same larva as an internal control. n=10 M4 NMJs from eight larvae for each genotype. Mean+s.e.m., paired two-tailed t-test, *** $P<0.001$. Shown here are high-magnification images, see Figure S1E for the overview of M4 NMJs. (**K and L**) High-magnification images (**K**) and quantification (**L**) of MARCM M4 NMJs co-stained with Brp (red) and GluRIIC (green, a marker for postsynaptic densities) antibodies show that some synapses at *PI31*$^{-/-}$ NMJs lost Brp puncta but maintained postsynaptic densities (white arrowheads). The GFP-positive neuron (shown in a pseudo magenta color) is *PI31*$^{-/-}$, whereas the GFP-negative neuron is *PI31*$^{+/-}$. n=7 M4 NMJs from seven larvae for each genotype. Mean+s.e.m., paired two-tailed t-test, ** $P<0.01$. See also Figure S1 and Table S1.

Figure 2. DYNLL1/2 are binding partners of PI31 in *Drosophila and mammalian cells*.

(**A**) Volcano plot of quantitative MS data of anti-HA-PI31 Co-IP (*Tub-GAL4, Tub-GAL80*^{ts} *>UAS-HA-PI31* flies) versus control Co-IP (*Tub-GAL4, Tub-GAL80*^{ts} flies). Biological triplicates were conducted and analyzed. The cutoff line for significance is *P*-value<0.01(-$\log_{10}$P >2) and fold difference>4 ($\log_2$fold difference >2 or <-2). PI31, dDYNLL1/2, 20S proteasome subunits and other statistically significant proteins are labeled in green, red, blue and pink, respectively; whereas ribosomal proteins and other statistically insignificant proteins are labeled in black and grey, respectively. The size of dots roughly indicates the amount of a given protein detected by MS. dDYNLL1/2 are among the statistically most significant interactors of PI31, along with 20S proteasome subunits which were previously identified as PI31 interacting proteins(Bader et al., 2011; Cho-Park and Steller, 2013; McCutchen-Maloney et al., 2000; Yashiroda et al., 2015). (**B and C**) The interaction between PI31 and dDYNLL1/2 was validated by Co-IP-Western blot analyses with *Tub-GAL4, Tub-GAL80*^{ts}*>HA-PI31* flies (**B**) and *HA-PI31*$^{Knock\text{-}in}$ flies (**C**). Human DYNLL1 and proteasome subunit α7 antibodies that cross-reacts with fly proteins were used for Western blotting (Bader et al., 2011; Kreko-Pierce and Eaton, 2017)

(**D**) Reciprocal Co-IP using FLAG-dDYNLL1 as the bait further confirmed the interaction between PI31 and dDYNLL1.
(**E**) The interaction between PI31 and DYNLL1/2 is conserved in mouse embryonic fibroblasts (MEFs).
See also Figure S2 and S3.

Figure 3. A conserved serine phosphorylation of PI31 involves in its interaction with DYNLL1/2.
(A and B) High resolution/high mass accuracy tandem MS spectra for the phospho-peptides of *Drosophila* **(A)** and human **(B)** PI31. Both peptides were matched with mass accuracy of <1ppm. Peptide information: *Drosophila*, EVTTQTTNSPRPIGSDPDPLR, +3, m/z: 787.70709 Da (-0.67 ppm); human, ANVSSPHREFPPATAR, +3, m/z: 606.28833 Da (-0.73 ppm).
(C) Alignment of the phosphorylation motifs of PI31 in *Drosophila*, human and mouse, indicating that PI31 is phosphorylated on a conserved serine residue.
(D) Volcano plot of quantitative MS data of anti-HA-PI31^{S168A} Co-IP (*Tub-GAL4, Tub-GAL80^{ts} >UAS-HA-PI3^{S168A}* flies) versus anti-HA-PI31^{WT} Co-IP (*Tub-GAL4, Tub-GAL80^{ts} >UAS-HA-PI3^{WT}* flies). Biological triplicates were conducted and analyzed. PI31, dDYNLL1/2, and 20S proteasome subunits are labeled in green, red, and blue, respectively. The size of dots roughly indicates the amount of a given protein detected by MS. The result indicates that dDYNLL1/2 are the statistically most significant interactor affected by the non-phosphorable mutation of PI31, whereas the binding of 20S proteasome subunits to PI31 is not dramatically changed.

Figure 4. The phosphorylation of PI31 regulates its direct interaction with dDYNLL1/2.
(A and B) Co-IP-Western blot analysis showed that the non-phosphorable mutation of PI31 (S168A) largely diminished its interaction with dDYNLL1/2 in S2 cells **(A)** and transgenic flies **(B)**.
(C) Reciprocal Co-IP using FLAG-dDYNLL1 as the bait confirmed that the PI31-dDYNLL1 interaction was phosphorylation-dependent.

(D) GST-Pull down assay indicates that the PI31 phosphorylation promotes its direct interaction with dDYNLL1. All recombinant proteins were produced in *E. coli.* Ponceau S that stains total proteins was used to assess the amount and purity of recombinant GST and GST-PI31 proteins. Anti-FLAG antibody was used to detect FLAG-dDYNLL1 pulled down by different forms of GST-PI31 proteins. The results demonstrate that purified GST-PI31 but not GST can pull down recombinant FLAG-dDYNLL1, indicating that PI31 and dDYNLL1/Ctp directly bind to each other. Importantly, this direct interaction was dramatically enhanced by two phosphor-mimetic mutations of PI31 (GST- PI31-S168D and GST- PI31-S168E), suggesting that the pS168 of PI31 promotes the interaction.

Figure 5. dDYNLL1/Ctp forms a protein complex with proteasomes

(A) Anti-FLAG-dDYNLL1 Co-IP and MS analysis reveal that dDYNLL1/Ctp forms a protein complex with proteasomes. S2 cells expressing FLAG-dDYNLL1 were collected for anti-FLAG Co-IP experiments. Shown here is a volcano plot of label-free quantitative MS analysis of anti-FLAG Co-IP experiments. Biological triplicates were conducted and analyzed. The cutoff line for significance is *P*-value<0.01($-\log_{10}P > 2$) and fold difference>4 ($\log_2$fold difference >2 or <-2). dDYNLL1/2, PI31, 20S proteasome subunits and other statistically significant proteins are labeled in red, green, blue and pink, respectively; whereas ribosomal proteins and other statistically insignificant proteins are labeled in black and grey, respectively. The size of dots roughly indicates the amount of a given protein detected by MS.

(B) Western blot analysis of anti-FLAG-dDYNLL1 Co-IP samples indicated the existence of dDYNLL1/Ctp-proteasome complexes. S2 cells expressing FLAG-dDYNLL1 were collected for anti-FLAG Co-IP experiments. Anti-α7, an antibody towards a 20S proteasome subunit α7 was used to detect proteasomes. This result is consistent with the MS data shown in (A) and shows that dDYNLL1/Ctp forms a protein complex with proteasomes.

Figure 6. PI31 promotes the formation of dDYNLL1/Ctp-proteasome complexes.

(A) PI31 promotes the formation of dDYNLL1/Ctp-proteasome complexes in S2 cells.

FLAG-dDYNLL1 was expressed in S2 cells with or without different forms of HA-PI31. After anti-FLAG Co-IP, Western blot analysis using proteasome subunit α7 antibody was conducted to detect proteasomes pulled down by dDYNLL1. The results indicate that PI31 can dramatically increase the amount of proteasomes bound to dDYNLL1/Ctp, and this ability is largely diminished by the non-phosphorable mutation (S168A).
(B) PI31 promotes the formation of dDYNLL1/Ctp-proteasome complexes *in vitro*. Recombinant FLAG-dDYNLL1 was expressed in *E. coli* and bound to anti-FLAG magnetic beads. Next, purified bovine 20S proteasomes were added alone, or with GST or different forms of GST-PI31 proteins, which were expressed and purified from *E.coli.* GST-PI31, but not GST, was able to load 20S proteasomes onto dDYNLL1/Ctp *in vitro*, and this ability can be further promoted by two phosphor-mimetic mutations (S168D and S168E). The upper panel depicts a schematic model for the *in vitro* binding assay, and representative results from Western Blot analyses are shown on the bottom.

Figure 7. PI31 and its phosphorylation are required for axonal transport of proteasomes in motor neurons.
(A) Representative kymographs of Prosβ5-RFP motility in motor neurons of wild-type *PI31*$^{-/-}$ 3rd-instar, and *PI31*^{S168A} *knock-in* larvae. *Prosβ5-RFP* expression was driven by *R94G06-GAL4*, a motor neuron-specific driver (See Figure S1). The kymographs were generated from 70-second live imaging (100 frames). The x-axis represents distance, while the y-axis represents time. Stationary particles appear as vertical lines, whereas motile particles appear as diagonal lines on kymographs. The directions of anterograde and retrograde movement are indicated on top of the kymographs. The results show that loss of PI31 causes severely reduced motility of proteasomes in axons, and PI31^{S168A} reduces the retrograde transport of proteasomes and increases the reversing movement. The red asterisks indicate the tracks of three proteasome particles that changed their moving direction and showed reversing movement during living imaging.
(B) Quantification of proteasome movement. Shown are the fractions of Prosβ5-RFP particles that moved in anterograde direction, retrograde direction, appeared stationary and reversely moved in axons of wild-type, *PI31*$^{-/-}$ and *PI31*^{S168A} *knock-in* motor neurons. Mean + s.e.m. n=7 larvae for wild-type, n=12 larvae for *PI31*$^{-/-}$, and n=7 larvae for

PI31^{S168A} knock-in. One-way Anova with Tukey's multiple comparison test. ****P<0.001*, ** *P<0.01*. In axons of *PI31$^{-/-}$* motor neurons, both anterograde and retrograde movements of proteasome particles were drastically reduced, while the portion of stationary proteasome particles increased accordingly; PI31^{S168A} reduces the retrograde transport of proteasomes and increases the reversing movement.

(C and D) Representative fluorescence images (**C**) and kymographs (**D**) of cultured mouse DRG neurons expressing mCerulean-mPI31 (green) and α4-mCherry (red) demonstrate that they extensively co-localize and move together in axons. The kymographs were generated from a 140-second live imaging experiment (70 frames). See also Figure S4 and Movie S1-4.

Figure 8. p38 MAPK can phosphorylate PI31.

(A) A candidate-based kinase RNAi screen identified p38β MAPK as a kinase that can phosphorylate PI31 at S168. *Tub-GAL4, Tub-GAL80^{ts}>UAS-HA-PI31* flies were crossed with RNAi transgenic fly strains targeting each MAPK or CDK family kinases. HA-PI31 protein was pulled down, digested and the peptides containing the phosphorylated and non-phosphorylated S168 were targeted and measured in a PRM experiment (EVTTQTTN^{168}SPRPIGSDPDPLR). Phosphopeptide signal versus total signal was used to estimate the phosphorylation occupancy percentage (POP). The POP distribution of kinase RNAi strains is presented as a box plot with the following percentiles: 10% and 90% (bottom and top whiskers), 25% and 75% (bottom and top of box) and 50% (middle line). The POPs for control RNAi strains are shown as grey dots, and the POPs for replicates of the P38β MAPK RNAi are shown as red and yellow dots, suggesting ~50% decrease of phosphorylation.

(B) The pS153 of hPI31 increases under osmotic stress, a classical condition to activate p38 MAPK. HEK293 cells were treated with 0.3M sorbitol for indicated time.

(C) The increase of pS153-hPI31 under osmotic stress was blocked by p38 MAPK inhibitor. HEK293 cells were pretreated with the indicated compounds (SB203580, SB202190 and BIRB796) at 10 μM for 2 hours, followed by the treatment of 0.3M sorbitol for 1 hour. The results show that SB203580 and SB202190, which inhibit p38α and p38β, only mildly suppress pS153-hPI31, whereas BIRB796 that targets all four

isoforms of p38MAPK can dramatically reduce the pS153-hPI31. This data suggests that PI31 phosphorylation requires p38 MAPK activity.

(D) *In vitro* kinase assay using recombinant proteins generated in E coli. demonstrates that p38 MAPK can directly phosphorylate hPI31 at S153. The asterisk indicates a C-terminal truncated form of PI31, which can not be visualized by the PI31 (total) antibody that recognizes the C-terminal region(Bader et al., 2011).

See also Figure S5.

Figure 9. Model for PI31-mediated transport of proteasomes in axons.

Proteasomes can move rapidly along microtubules, allowing them to fulfill dynamic local demands for protein degradation in different cellular compartments(DiAntonio et al., 2001; Hegde et al., 2014; Hsu et al., 2015; Kreko-Pierce and Eaton, 2017; Watts et al., 2003; Zhao et al., 2003). PI31 binds directly to both proteasomes and dynein light chain LC8-type proteins (DYNLL1/2), which play a key role in microtubule-dependent transport(Bader et al., 2011; Cho-Park and Steller, 2013; Chu-Ping et al., 1992; Hsu et al., 2015; Kreko-Pierce and Eaton, 2017). Inactivation of PI31 severely reduces proteasome movement in *Drosophila* and leads to the accumulation of Poly-Ub aggregates in the periphery of neurons. This suggests that PI31 functions as a direct adaptor to couple proteasomes to microtubule-based motors. PI31 phosphorylation by the stress-activated p38 MAPK can directly regulate the PI31-dDYNLL1 interaction and thereby modulate proteasome transport in axons. This may serve to dynamically adjust the spatio-temporal distribution of proteasomes in response to stress and thereby adjust the protein degradation capacity of cells to match changing demands for protein breakdown. If this mechanism is impaired, mis-regulation of proteasome distribution occurs and leads to a failure of local protein degradation.

Methods

Fly husbandry and strains

All flies were raised on standard molasses formulation food at 25°C with a 12-hour light/12-hour dark cycle. The following fly strains were used: *R94G06-GAL4* (Janelia GAL4 collection, Bloomington Drosophila Stock Center, BDSC#40701, RRID:BDSC_40701) (Pfeiffer et al., 2008), *UAS-mCD8-mCherry* (BDSC #27392, RRID:BDSC_27392), *UAS-HA-PI31* (2nd chromosome)(Bader et al., 2011), $PI31^{-/-}$(Bader et al., 2011), $hsp70\text{-}FLP^{1}$, *FRT42D tubP-GAL80* (BDSC #9917, RRID:BDSC_9917), *D42-GAL4* (BDSC # 8816, RRID:BDSC_8816), *UAS-IVS-myr::GFP* (BDSC #32197, RRID:BDSC_32197) (Pfeiffer et al., 2010), *tubP-GAL4* (BDSC # 5138, RRID:BDSC_5138), $tubP\text{-}GAL80^{ts}$ (BDSC #7018, RRID:BDSC_7018), *Nrv2-GAL4 UAS-GFP* (BDSC #6794, RRID:BDSC_6794), *UAS- PI31 RNAi*^{KK105476} (Vienna Drosophila Resource Center, #105476, RRID:FlyBase_FBst0473568) and *UAS-Prosβ5-RFP*(Kreko-Pierce and Eaton, 2017) (kindly provided by Dr. Benjamin A. Eaton, University of Texas). *UAS-HA-PI31-WT* $^{attP_ZH\text{-}68E}$, *UAS-HA-PI31-S168A* $^{attP_ZH\text{-}68E}$, *UAS-HA-PI31-S168D* $^{attP_ZH\text{-}68E}$, *HA-PI31*$^{Knock\text{-}in}$ and $PI31^{S168A}$ *knock-in* (this study, see below).

Fly genotypes for each figure, table and movie are listed below:

Figure 1A. *w; UAS-HA-PI31/+; R94G06-GAL4/+.*

Figure 1B-H and Figure S1B-E. WT: *yw; +/+; +/+.* $PI31^{-/-}$: *w;* $PI31^{\Delta}/PI31^{\Delta}$*;+/+.*

Figure 1I-L. *yw,* $hsp70\text{-}FLP^{1}$*; FRT42D, tubP-GAL80/FRT42D,* $PI31^{\Delta}$*; UAS- IVS-myr::GFP/D42-GAL4.*

Figure 2A and 2B. Control: *yw; +/+; tubP-GAL4,* $tubP\text{-}GAL80^{ts}$ */+.*

HA-PI31: *w; +/+; tubP-GAL4,* $tubP\text{-}GAL80^{ts}$*/UAS-HA-PI31-WT* $^{attP_ZH\text{-}68E}$.

Figure 2C and Figure S3. Control: *yw; +/+; +/+.*

HA-PI31$^{Knock\text{-}in}$: *w; HA-PI31*$^{Knock\text{-}in}$*/ HA-PI31*$^{Knock\text{-}in}$ *; +/+.*

Figure 3A. *w; +/+; tubP-GAL4,* $tubP\text{-}GAL80^{ts}$*/UAS-HA-PI31-WT* $^{attP_ZH\text{-}68E}$.

Figure 3D.

HA-PI31-WT: *w; +/+; tubP-GAL4,* $tubP\text{-}GAL80^{ts}$*/UAS-HA-PI31-WT* $^{attP_ZH\text{-}68E}$.

HA-PI31-S168A: *w; +/+; tubP-GAL4,* $tubP\text{-}GAL80^{ts}$*/UAS-HA-PI31-S168A* $^{attP_ZH\text{-}68E}$.

Figure 4B.

HA-PI31-WT: *w; +/+; tubP-GAL4, tubP-GAL80^{ts}/UAS-HA-PI31-WT $^{attP_ZH-68E}$.*

HA-PI31-S168A: *w; +/+; tubP-GAL4, tubP-GAL80^{ts}/UAS-HA-PI31-S168A $^{attP_ZH-68E}$.*

HA-PI31-S168D: *w; +/+; tubP-GAL4, tubP-GAL80^{ts}/UAS-HA-PI31-S168D $^{attP_ZH-68E}$.*

Figure 7A, 7B and Movies S1-3.

WT: *w; +/+; R94G06-GAL4, UAS-Prosβ5-RFP/R94G06-GAL4, UAS-Prosβ5-RFP.*

PI31$^{-/-}$: *w; PI31$^{\Delta}$/ PI31$^{\Delta}$; R94G06-GAL4, UAS-Prosβ5-RFP/R94G06-GAL4, UAS-Prosβ5-RFP.*

PI31^{S168A} knock-in: w; PI31^{S168A}/PI31^{S168A}; R94G06-GAL4, UAS-Prosβ5-RFP/R94G06-GAL4, UAS-Prosβ5-RFP.

Figure 8A. F1 non-Tb flies from the cross of *w; UAS-HA-PI31/UAS-HA-PI31; tubP-GAL4, tubP-GAL80^{ts}/TM6B, Tb* with kinase RNAi transgenic lines.

Figure S1. *w; +/+; R94G06-GAL4/UAS-mCD8-mCherry.*

Figure S4C. *w; PI31^{S168A}/+;+/+.*

Table S1. *Nrv2-GAL4*: *w;+/+; Nrv2-GAL4, UAS-GFP/Nrv2-GAL4, UAS-GFP.*

PI31 RNAi: *w; PI31 RNAi^{KK105476}/PI31 RNAi^{KK105476}.*

Nrv2>PI31 RNAi: *w; PI31 RNAi^{KK105476}/PI31 RNAi^{KK105476}; Nrv2-GAL4, UAS-GFP/Nrv2-GAL4, UAS-GFP.*

Constructs

The gRNA constructs for making *HA-PI31$^{Knock\text{-}in}$* and *PI31^{S168A} knock-in* fly strains were generated by annealing of two ssDNA oligonucleotides (ssODN) together and inserting the annealed products into the BbsI site of pCFD3-dU6:3gRNA vector (Port et al., 2014) (a gift from Dr. Simon Bullock, Addgene#49410). Listed are the ssODN sequences:

HA-PI31$^{Knock\text{-}in}$_F: GTCGAGTCGACCCACTTTCCATTG;

HA-PI31$^{Knock\text{-}in}$_R: AAACCAATGGAAAGTGGGTCGACT;

PI31^{S168A} knock-in_F: GTCGTCCAATGGGGCGTGGTGAGT;

PI31^{S168A} knock-in_R: AAACACTCACCACGCCCCATTGGA.

To generate S2 cell vectors to express HA-PI31 and FLAG-dDYNLL1, the HA-PI31 fragment was cut from pcDNA3-HA-PI31(Bader et al., 2011) using EcoRI and XhoI (New England Biolabs), and the FLAG-dDYNLL1 was cloned from a yw cDNA library by PCR and the FLAG-tag sequence was added on the forward primer in frame with the dDYNLL1 coding sequence (CDS). HA-PI31(EcoRI/XhoI) and FLAG-dDYNLL1(EcoRI/XbaI) fragments were inserted into the S2-cell expression vector pAc5.1/V5-His-A(Thermo Fisher Scientific, V411020).

To generate the S168 point mutation transgenic fly strains (*UAS-HA-PI31-WT* $^{attP_ZH\text{-}68E}$, *UAS-HA-PI31-S168A* $^{attP_ZH\text{-}68E}$, *UAS-HA-PI31-S168D* $^{attP_ZH\text{-}68E}$), we first mutated the site on pcDNA3-HA-PI31(Bader et al., 2011) through PCR-based site directed mutagenesis. The PCR primers we used are:
S168A_F: CCACGCAGACGACCAACGCCCCACGCCCCATTGGATC;
S168A_R: GATCCAATGGGGCGTGGGGCGTTGGTCGTCTGCGTGG;
S168D_F: CCACGCAGACGACCAACGATCCACGCCCCATTGGATCG;
S168D_R: CGATCCAATGGGGCGTGGATCGTTGGTCGTCTGCGTGG.
After PCR, the template DNA was removed by DpnI treatment. The mutated clones were isolated by Sanger sequencing, and sub-cloned into pUAST-attB vector with EcoRI and XhoI restriction enzymes (New England Biolabs)(Bischof et al., 2007).

To generate S2 cell vectors to express HA-PI31 S168 point mutants, the above mutants are sub-cloned into pAc5.1/V5-His-A (Thermo Fisher Scientific, V411020) with EcoRI and XhoI restriction enzymes (New England Biolabs).

To generate *E coli.* vectors to recombinantly express different forms of GST-HA-PI31 and FLAG-dDYNLL1, the HA-PI31-WT, -S168A, -S168D and -S168E fragments were cut from pcDNA3-HA-PI31 vectors using EcoRI and XhoI and inserted into the pGEX-4T1 vector (GE Healthcare, #28954549) to generate pGEX-4T1-PI31 clones; the FLAG-dDYNLL1 fragment was produced by PCR using pAc5.1A-FLAG-dDYNLL1 as the template, digested with NcoI and EcoRI (New England Biolabs), and inserted into pET28a vector (Novagen, #69864-3) to generate the pET28a-FLAG-dDYNLL1 clone.

Mouse PI31 (mPI31) CDS was cloned from a cDNA library of mouse small intestine, which was generated by Superscript III First Strand Synthesis Kit (Thermo Fisher Scientific, #18080051) using oligo(dT) amplification, and inserted into the BstI/XmaI sites of pLVX-EF1a-AcGFP-C1 vector (Clontech, #631984). The lentivirus was packaged by transfection of pLVX-EF1a-AcGFP-C1-mPI31, pMD2.G (a gift from Dr. Didier Trono, Addgene #12259) and psPAX2 (a gift from Dr. Didier Trono, Addgene #12260) into HEK293 cells, and collected 48 hours after transfection. Human PI31 (hPI31) CDS was cloned from a cDNA library of HEK293 cells, and inserted into pcDNA3.2/V5/GW/D-TOPO vector (Thermo Fisher Scientific, K244020) through TOPO cloning method (kindly provided by Dr. Park Cho-Park, University of Pennsylvania).

Mouse proteasome subunit α4 CDS was cloned from a mouse cDNA library, and mCherry CDS was subcloned from the mCherry-Mito-7 vector (Olenych et al., 2007) (a gift from Dr. Michael Davidson, Addgene #55102). The α4-mCherry cassette was inserted between the EcoRI/NotI sites of pCAGGS/ES vector. mCerulean CDS was amplified by PCR using mCerulean-N1 vector as the template (Koushik et al., 2006)(a gift from Dr. Steven Vogel, Addgene #27795), and mPI31 CDS was cloned from a mouse cDNA library. The mCerulean-mPI31 cassette was inserted between the EcoRI/NheI sites of pCAGGS/ES vector.

All the constructs were validated by Sanger sequencing (Genewiz).

Antibody production

To generate a polyclonal antibody against *Drosophila* PI31, GST-PI31 was expressed in BL21 Star (DE3) *E.coli* cells(Thermo Fisher Scientific, #C601003), and purified using Glutathione Sepharose 4B beads (GE Healthcare, #17-0756-01). The purified protein was injected into rabbits and the antisera were collected (Cocalico).

To generate the phosphorylation-specific antibody against pS153-hPI31, a phospho-peptide was synthesized (Figure S5A), conjugated to carrier proteins and

injected into rabbits (YenZym Antibodies, LLC). The elicited antiserum was first affinity-purified against the phospho-peptide. Bound antibodies were eluted and further affinity-absorbed against the non-phosphorylated peptide counterpart to remove antibodies recognizing the other parts of the peptide instead of the phosphorylation site.

Generation of MARCM clones

PI31$^{-/-}$ mutant clones were made using the mosaic analysis with a repressible cell marker (MARCM) system(Wu and Luo, 2006). The fly genotype is: *yw, hsp70-FLP*^{1}*; FRT42D, tubP-GAL80/FRT42D, PI31*$^{\Delta}$*; UAS- IVS-myr::GFP/D42-GAL4*. The eggs were laid on fly food at 25°C. The 0-6-hour embryos were heat-shocked at 37°C for 30mins followed by recovery at 25 °C for 30mins, and then heat-shocked again at 37°C for 45mins. The wandering 3rd-instar larvae with the appropriate genotype were dissected and proceeded for immunostaining.

Generation of *HA-PI31*$^{Knock\text{-}in}$ and *PI31*^{S168A} *knock-in* fly strains

The off-target effect of gRNAs were assessed by CRISPR target finder (http://tools.flycrispr.molbio.wisc.edu/targetFinder/) (Gratz et al., 2014) and E-CRISPR (www.e-crisp.org/E-CRISP/)(Heigwer et al., 2014). The selected sequences (HA-PI31$^{Knock\text{-}in}$:AGTCGACCCACTTTCCATTG , on the "-" strand; PI31^{S168A} knock-in: TCCAATGGGGCGTGGTGAGT, on the "-" strand) were cloned into pCFD3-dU6:3gRNA vector as described above(Port et al., 2014). ssODN, which serve as the donor template for HDR-mediated recombination, was designed with ~50nt homology arm on each side, and synthesized (IDT). The sequences of the ssODN are:

HA-PI31$^{Knock\text{-}in}$:

CTTGTACAGCAGATCCCAACCGTAAAAGAAATCGCCCGTCTTGGCAGTCGAC
CCACTTTCGCCACCGCCGCTAGCATAGTCGGGCACATCATATGGGTACATTGC
GGCCACCGATAATCCTTTACAAAATCTGGGTGGGAGTAAACAGAACGAATGG
AAC;

PI31^{S168A} knock-in:

GTTCTTACCCGCCACGCCTTGGCTCGCCGATGCGCAAGGGATCTGGATCCGAT

CCAATGGGGCGTGGTGCGTTCGTCGTCTGCGTGGTAACTTCGCGCGAGTTTCC CGTGAATACAGGGTCTAGAAGCTC.

The pCFD3-dU6:3-PI31 gRNA constructs (final concentration 150ng/µl) and the donor template ssODN (final concentration 200ng/µl) were mixed together and injected into the *y, sc, v; +/+; nos-Cas9*^{attP2} fly (Ren et al., 2013). Knock-in flies were initially identified by PCR and then confirmed by Sanger sequencing (Genewiz).

Immunofluorescence

Wandering 3rd-instar larvae were pinned on a silicone petri dish, and dissected in HL3 saline. The fillet preparations were fixed in 4% paraformaldehyde/PBS for 20mins. After washing with PBS/0.1% Triton X-100 (PBST), the fillets were blocked in 5% NGS/0.2% BSA/PBST, followed by incubation with primary antibodies overnight at 4°C. After washing for 3 times with 0.2%BSA/PBST, the secondary antibodies were applied at room temperature for 3 hours. The fillets were washed 4 times and proceeded for mounting and examination on a confocal microscope (LSM780, Zeiss). The following antibodies were used: chicken anti-mCherry (1:500, Novus, #NBP2-25158, RRID:AB_2636881), rat anti-HA (1:100, clone 3F10, Sigma-Aldrich, #11867423001, RRID:AB_390918), mouse anti-ubiquitin conjugates (1:500, clone FK2, Enzo, #PW8810, RRID:AB_10541840), mouse anti-Brp (1:300, clone nc82, Developmental Studies Hybridoma Bank, #nc82, RRID:AB_2314866), chicken anti-GFP (1:1000, Aves Labs, #GFP-1020, RRID:AB_10000240), rabbit anti-GluRIIC(Marrus et al., 2004) (1:1000, kindly provided by Dr. Aaron DiAntonio, Washington University in St. Louis, RRID:AB_2568754), goat anti-rat-Alexa 488(1:500, Jackson ImmunoResearch, #112-545-167, RRID:AB_2338362), goat anti-mouse-Alexa 488 plus (1:500, Thermo Fisher Scientific, #A32723, RRID:AB_2633275), goat anti-chicken-Alexa 488(1:500, Jackson ImmunoResearch, #103-545-155, RRID:AB_2337390), goat anti-chicken-Cy3(1:500, Jackson ImmunoResearch, #103-165-155, RRID:AB_2337386), goat anti-mouse-Alexa 568(1:500, Thermo Fisher Scientific, #A11031, RRID:AB_144696), goat anti-HRP-Cy3(1:3000, Jackson ImmunoResearch, #123-165-021, RRID:AB_2338959), goat anti-rabbit-Alexa 633(1:500, Thermo Fisher Scientific, #A21071, RRID:AB_2535732), and goat anti-HRP-Alexa 647(1:300, Jackson ImmunoResearch, #123-605-021,

RRID:AB_2338967). Quantification of puncta number and intensity of Poly-Ub proteins was done with Fiji software(Schindelin et al., 2012), and Fiji and Imaris (Bitplane) softwares were used for quantification of numbers and volume of Brp puncta.

Co-Immunoprecipitation (Co-IP)

For the Co-IP experiments shown in Figure 2A, 2B, 3A, 3D, 4B and 8A, *tubP-GAL4, tubP-GAL80*^{ts} flies were crossed with indicated forms of *UAS-HA-PI31* or *yw* (as control) flies and raised at 25°C. The 0-3-day-old F1 progenies were collected and moved to 29°C for 6 days. Three-hundred male flies were collected and homogenized in 1.5ml buffer A [50mM Tris-HCl (pH7.5), 137mM NaCl, 0.25% NP-40, protease inhibitor cocktail (Roche, #11873580001) and phosphatase inhibitor cocktail (Roche, #04906837001)]. After centrifuged at 20000g for 15mins and filtered through a low-protein binding 0.45µm PVDF membrane syringe filter (Millipore, #SLHVX13NL), the extracts were incubated with 30µl mouse anti-HA agarose beads (clone HA-7, Sigma-Aldrich, #A2095, RRID:AB_257974) at 4°C for 3 hours. After six washes in buffer A and two additional washes in buffer A without NP-40 and protease and phosphatase inhibitors, the beads were eluted in 30µl 0.1M glycine (pH2.5) at room temperature for 10mins. The eluted proteins were taken either for mass spectrometry (MS) analysis (Figure 2A, 3A, 3D and 8A) or for Western Blot analysis (Figure 2B and 4B).

For the Co-IP experiment shown in Figure 2C, 150 3-day old male *HA-PI31*$^{Knock\text{-}in}$ flies and *yw* flies (as control) were collected separately and homogenized in 1ml buffer A with 50U/ml DNase I (Thermo Fisher Scientific, #18047019). After centrifuged at 20000g for 15mins, sonicated briefly to break genomic DNAs, and filtered through a 0.45µm syringe filter, the extracts were incubated with 30µl mouse anti-HA magnetic beads (Thermo Fisher Scientific, #88836) at 4°C for 3 hours. After five washes in buffer A and two additional washes in buffer A without NP-40 and protease and phosphatase inhibitors, the beads were eluted in 30µl 500µg/ml HA peptide (Thermo Fisher Scientific, #26184) at 37°C for 30mins. The eluted proteins were analyzed by Western blotting.

For the IP or Co-IP experiments shown in Figure 2D, 2E, 3B, 4A, 4C, 5B, 6A, S2C, S2D, and S5B, 10cm-plate cultures of indicated cell lines were transfected/infected with indicated constructs using TransIT-Insect transfection reagent (Mirus, #MIR6100) for S2 cells (RRID:CVCL_Z232), Lipofectamine 2000 transfection reagent (Thermo Fisher Scientific, #11668-019) for HEK293 cells(RRID:CVCL_0045) and lentivirus for primary MEFs, respectively. After 48 hours for the transfected cells or 7 days for the infected MEFs, the cell cultures were rinsed in cold PBS, collected, and resuspended in 0.6ml buffer A. Lysis was facilitated by freeze/thaw for three times. After centrifugation at 20000g for 15mins and filtration through a 0.45µm syringe filter, the extracts were incubated with 30µl mouse anti-HA agarose beads (clone HA-7, Sigma-Aldrich, #A2095, RRID:AB_257974), or 30µl mouse anti-FLAG magnetic beads (clone M2, Sigma-Aldrich, #M8823, RRID:AB_2637089), or 30µl GFP-Trap agarose beads (Chromotek, gta-20, RRID:AB_2631357) at 4°C for 3 hours. For Western blot analysis, the beads were washed in buffer A for six times and then were eluted in 30µl 1.5XSDS-PAGE sample buffer by boiling at 95°C for 5mins. For MS analysis (Figure 3A), the beads were washed in buffer A for five times and then in buffer A without NP-40 and protease and phosphatase inhibitors for two times, followed by the elution in 30µl 0.1M glycine (pH2.5) at room temperature for 10mins. For Figure S5B, after five washes in buffer A and two additional washes in buffer A without NP-40 and protease and phosphatase inhibitors, the beads were proceeded for phosphatase assay (see below).

For the Co-IP experiment shown in Figure 5A, 10-cm plate cultures of S2 cells were transected with 15µg pAc5.1A-FLAG-dDYNLL1 or pAc5.1A empty vector (as control) constructs using TransIT-Insect transfection reagent. After 48 hours, the cells were rinsed, collected and resuspended in 600µl buffer A, and lysis was facilitated by freeze/thaw for three times. After centrifugation at 20000g for 15mins and filtration through a 0.45µm syringe filter, the extracts were incubated with 30µl mouse anti-FLAG magnetic beads (clone M2, Sigma-Aldrich, #M8823, RRID:AB_2637089) at 4°C for 3 hours. After six washes in buffer A and two additional washes in buffer A without NP-40 and protease and phosphatase inhibitors, the beads were eluted in 30µl 300 µg/ml 3XFLAG peptide (Sigma-Aldrich, #F4799) at 4°C for 45mins. The eluted proteins were

run on a SDS-PAGE gel for ~1cm to remove the 3XFLAG peptide. Finally, the gel was cut for MS analysis. Biological triplicates of the Co-IP were used for quantification.

For the Co-IP experiment shown in Figure S3, eight hundreds of 3-day-old male *HA-PI31*$^{Knock\text{-}in}$ flies and *yw* flies (as control) were collected separately and homogenized in 5ml buffer B [25mM HEPES (pH7.5), 100mM NaCl, 5mM MgCl2, 2mM ATP, 10% glycerol, 0.25% NP-40, protease inhibitor cocktail and phosphatase inhibitor cocktail] with 50U/ml DNase I (Thermo Fisher Scientific, #18047019). After centrifugation at 20000g for 15mins, lysates were sonicated briefly to break genomic DNA and filtered through a 0.45µm syringe filter, and then the extracts were incubated with 200µl mouse anti-HA magnetic beads (Thermo Fisher Scientific, #88836) at 4°C for 3 hours. After five washes in buffer B and two additional washes in buffer C [25mM HEPES (pH7.5), 150mM NaCl, 5mM $MgCl_2$, 2mM ATP, 10% glycerol], the beads were eluted by 200µl 500µg/ml HA peptide in buffer C at 37°C for 30mins. The eluted proteins were concentrated 5X with 10KDa-cutoff Amicon centrifugal filter unit (Millipore, #UFC501024), and analyzed by native gels and Western blotting.

Mass spectrometry analysis

Glycine (0.1M, pH2.5) eluted samples (Figure 2A, 3A, 3B, 3D and 8A) were dried in Speedvac concentrator (Thermo Fisher Scientific) and dissolved in 8M urea, 0.1M ammonium bicarbonate, and 10mM DTT. After reduction, cysteines were alkylated in 30mM iodoacetamide. The proteins were digested in less than 4M urea by endoproteinase LysC (Wako Chemicals) followed by digestion with Trypsin Gold (Promega) in less than 2M urea. FLAG-peptide eluted samples (Figure 5A) were cleaned up using SDS-PAGE, reduced (10mM DTT) and alkylated (30mM iodoacetamide), followed by digestion with a cocktail of LysC and Trypsin Gold. Digestions were halted by adding trifluoroacetic acid (TFA) and digests were desalted and analyzed by reversed phase nano-LC-MS/MS using either a Fusion Lumos or a Q-Exactive Plus (Thermo Fisher Scientific) both operated in high/high mode(Rappsilber et al., 2007).

Data were searched and quantified against a Uniprot's *Drosophila* database (21,945 sequences, March 2016) using Proteome Discoverer v1.4.0.288 (Thermo Fisher Scientific) combined with Mascot v2.5.1 (Matrix Science) and MaxQuant v1.6.0.13(Cox et al., 2014). Oxidation of methionine and protein N-terminal acetylation were allowed as variable modifications and all cysteines were treated as being carbamidomethylated. Peptide matches were filtered using a Percolator-calculated false discovery rate (FDR) of 1%(Kall et al., 2007). For the quantitative MaxQuant analysis, FDR thresholds for peptides and proteins were set at 2% and 1%, respectively.

Label Free Quantitation (LFQ) or intensity-based absolute quantification (iBAQ) were used for the identification and quantitation of binding partners(Cox et al., 2014; Schwanhausser et al., 2011). Data were processed using Perseus v1.6.0.7(Tyanova et al., 2016). In short, reverse matches and common contaminations were disregarded, and protein signals in minimum 2 out of 3 replicates for at least one condition was required. Data were validated by scatter plots, LFQ or iBAQ based principal component analysis (PCA) and distributions of LFQ or iBAQ values, and found comparable. T-tests were performed and proteins were considered as interesting hits if showing a difference of more than 4-linear folds and a p-value of less than 0.01.

GST pull-down assays

BL21 Star (DE3) competent *E.coli* cells were transformed with pGEX-4T1-PI31 vectors (-WT, -S168A, -S168D, and -S168E), pGEX-4T1 empty vector or pET28a-FLAG-dDYNLL1 vector. Single colonies were picked and cultured in 5ml LB, followed by an enlarged culture in 100ml LB. When OD_{600}≈0.4, IPTG was added to a final concentration of 0.3mM. After 4 hours, the bacteria were collected by centrifugation and rinsed by cold PBS. The bacteria were resuspended in 5ml cold PBS with protease inhibitor cocktail, lysed by sonication and centrifuged at 20000g for 15mins.

1ml pGEX-4T1 empty vector lysate or 1ml pGEX-4T1-PI31 lysate were incubated with 30µl Glutathione Sepharose 4B beads at 4°C for 3 hours. Then, the beads were washed with PBS for three times, followed by incubation with 1ml pET28a-FLAG-

dDYNLL1 lysate at 4°C for 3 hours. The beads were washed in buffer A for five times and in 50 mM Tris-HCl (pH 8.0) once. Elution was done by incubation of the beads in 30µl GST elution buffer [50 mM Tris-HCl (pH 8.0) and 20mM reduced glutathione (Sigma-Aldrich, #G4251)] at room temperature for 20mins. The eluted proteins were analyzed by SDS-PAGE and Western blot. Ponceau S (Sigma-Aldrich, #P7170) staining was used to assess purity and amount of GST and different forms of GST-PI31 proteins. Anti-FLAG-HRP (1:1000, Sigma-Aldrich, #A8592) was used to evaluate amount of FLAG-dDYNLL1 bound to GST or different forms of GST-PI31 proteins.

***In vitro* reconstitution of dDYNLL1-PI31-proteasome complex**

Six-milliliter lysate of BL21 Star (DE3) expressing pET28a-FLAG-dDYNLL1 was incubated with 200µl mouse anti-FLAG magnetic beads (clone M2, Sigma-Aldrich, #M8823, RRID:AB_2637089) at 4°C for 3 hours. After washed with buffer A for four times, the beads were split equally into six tubes. Then, 5µg purified bovine 20S proteasomes (UBPbio, #A1401), or 5µg GST+5µg purified bovine 20S proteasomes, or 5µg indicated forms of GST-PI31 proteins+5µg purified bovine 20S proteasomes were added to the six tubes, respectively, and incubated at 4°C for 3 hours. After four washes in buffer A, the beads were eluted in 35µl 300µg/ml 3XFLAG peptide at 4°C for 45mins.

***In vitro* kinase assay**

Purified recombinant human p38α (MAPK14, GST-tagged, Thermo Fisher Scientific, #PV3304), p38β (MAPK11, His-tagged, Thermo Fisher Scientific, #PV3679), p38γ (MAPK12, His-tagged Thermo Fisher Scientific, #PV3654), p38δ (MAPK13, His-tagged, Thermo Fisher Scientific, #PV3656) and hPI31 (UBPBio, #A3901) were used for *in vitro* kinase assay.

One microgram of hPI31 was incubated with 200ng indicated kinases in 30µl kinase assay buffer [20 mM Tris (pH 7.5), 2 mM DTT, 10 mM MgCl2, 200µM ATP, and phosphatase inhibitors] at 30°C for 30mins. The reaction was terminated by adding 15µl 3XSDS-PAGE loading buffer and boiling at 95°C for 5mins.

***In vitro* phosphatase assay**

To validate the specificity of p153-hPI31 antibody, HA-hPI31 was expressed in HEK293 cells and IP with anti-HA agarose beads (see the "Co-IP" section for details). After wash, the beads were split into three tubes. One was incubated with 50µl phosphatase assay buffer (50mM HEPES, 100mM NaCl, 2mM DTT, 0.01% Brij-35) as a control, one was treated with 400U Lambda protein phosphatase (Lambda PP, New England Biolabs, #P0753S) in 50µl phosphatase assay buffer, and the other one was treated with Lambda PP in the presence of phosphatase inhibitor cocktail(Roche, #04906837001). After incubated at 30°C for 30mins, the beads were precipitated and hPI31 proteins were eluted in 1XSDS-PAGE loading buffer and boiled at 95°C for 5mins.

Native gel assays

Protein complexes captured by anti-HA Co-IP using extracts of *yw* (as control) and *HA-PI31*$^{Knock\text{-}in}$ flies were eluted in buffer C with HA peptide under the native condition (see the "Co-IP" section for more details). The eluted proteins, as well as 15µg total lysates of *yw* and *HA-PI31*$^{Knock\text{-}in}$ flies (as inputs for the Co-IP experiment), were mixed with 2X native sample buffer (Bio-rad, #1610738), and loaded onto 3-8% Tris-acetate gels (Bio-rad, #3450131). Purified bovine 19S (UBPbio, #A1301), 20S (UBPbio, #A1401) and 26S (UBPbio, #A1201) proteasomes were also loaded onto the gels as standards to mark positions of different proteasome complexes. Electrophoresis was started with 50V for 1 hour in running buffer (90mM Tris, 90mM Boric Acid, 1mM EDTA, 2.5 mM MgCl2, 1mM ATP and 0.5mM DTT). After samples fully entered the gel, voltage was increased to 120V and ran 5 hours at 4°C. Then, proteins in the gels were transferred to PVDF membrane for Western Blot.

Western Blot Analysis

Proteins in SDS-PAGE gels or native gels were transferred onto 0.45µm Immobilon-P PVDF membranes (Millipore. #IPVH00010). The membranes were blocked with 5% non-fat milk in TBST [20mM Tris (pH7.5), 300mM NaCl, 0.1% Tween-20] at room temperature for 1 hour, followed by incubation with primary antibodies in 5% BSA/TBST at 4°C overnight. After washed for three times with TBST, the membranes

were incubated with HRP-conjugated secondary antibodies at room temperature for 1.5 hours. The membranes were washed for four times with TBST, and detection was performed with ECL reagent (GE Healthcare, #RPN2134) or SuperSignal West Femto Maximum Sensitivity Substrate (Thermo Fisher Scientific, # 34096). The following antibodies were used for Western blot: rabbit anti-DYNLL1/2(1:3000, clone EP1660Y, Abcam, #ab51603, RRID:AB_2093654), mouse anti-α7 (1:3000, clone MCP72, Enzo, # PW8110, RRID:AB_10538395), mouse anti-Rpt3 (1:3000, clone TBP7-27, Enzo, # PW8765, RRID:AB_10541726), rabbit anti-dPI31(1:5000), goat anti-hPI31(1:3000, Thermo Fisher Scientific, #PA5-18133, RRID:AB_10980800), rabbit anti-hPI31(1:3000, Abcam, #ab140497), rat anti-HA-HRP(1:3000, clone 3F10, Roche, #12013819001, RRID:AB_390917), mouse anti-FLAG-HRP(1:1000, clone M2, Sigma-Aldrich, #A8592, RRID:AB_439702), mouse anti-GFP-HRP(1:1000, clone B2, Santa Cruz Biotechnology, #sc-9996-HRP, RRID:AB_627695), rabbit anti-GST-HRP(1:1000, Abcam, #ab3416, RRID:AB_303783), donkey anti-rabbit-HRP(1:5000, Jackson ImmunoResearch, #711-035-152, RRID:AB_10015282), donkey anti-mouse-HRP(1:5000, Jackson ImmunoResearch, #715-035-150, RRID:AB_2340770), goat anti-mouse Fc-HRP(1:3000, Thermo Fisher Scientific, #31437, RRID:AB_228295).

Live imaging

For analysis of proteasome transport in axons of *Drosophila* motor neurons, wandering 3rd-instar larvae of *R94G06-GAL4>Prosβ5-RFP* (as control), *PI31*$^{-/-}$*, R94G06-GAL4>Prosβ5-RFP and PI31*^{S168A}*, R94G06-GAL4>Prosβ5-RFP* were dissected in HL3 saline supplemented with 7mM L-glutamic acid, and flipped the inside out to expose motor neuron axons. The larval preparations were mounted on a microscope slide with coverslip bridges to avoid crash of tissues. Live imaging was done on a 60X silicone oil objective lens (NA1.3, Olympus) of inverted Olympus IX-70 microscope equipped with Evolve-512 EMCCD camera (Photometrics). Images were captured using a 500-ms exposure at 1.4 Hz, and each recording consisted of 100 frames in 70 seconds. Kymographs were generated and velocities of each proteasome particle were calculated using ImageJ with the “Multiple Kymograph” and “Walking Average” plugins. All particles were picked and tracked by the software.

For live imaging of α4-mCherry and mCerulean–PI31 in mouse DRG neuron cultures, DRGs were dissected from E13 mouse embryos (CD-1 IGS pregnant mouse, Charles River, #022, RRID:IMSR_CRL:22) and dissociated to single cell suspension using Trypsin. Dissociated sensory neurons were transfected with pCAGGS/ES-α4-mCherry and pCAGGS/ES-mCerulean–mPI31 plasmids using the Neon transfection system (Thermo Fisher Scientific, MPK5000) at 1400 V, 20 ms, and 1 pulse. After transfection, $5X10^5$ neurons were centrifuged, resuspended in 9µl growth medium [Neurobasal medium (Thermo Fisher Scientific, #21103049), B-27 (Thermo Fisher Scientific, #17504044), penicillin-streptomycin(Thermo Fisher Scientific, #15140122) with 12.5ng/ml mouse growth factor 2.5S (NGF, Alomone Labs, #N-100)] and transferred to 15µl growth medium as a hanging drop overnight to form cell aggregates. Aggregates were cut into four pieces, plated on Poly-D-Lysine (Sigma-Aldrich, #P6407)/Laminin (Sigma-Aldrich, #L2020)-coated 8-well µ-Slide (ibidi, # 80826) and cultured for additional 24-48 hours. Before imaging, culture medium was changed to Hibernate E low fluorescence media (BrainBits, #HELF) supplemented with B27 and NGF, in order to maintain cells in ambient CO_2 levels. Images were taken on a 60X silicone oil objective lens (NA1.3, Olympus) of inverted Olympus IX-70 microscope equipped with Evolve-512 EMCCD camera (Photometrics) and with a heating chamber at 37°C, at 0.5Hz for 1-3 minutes.

Supplementary Information

Supplemental Information includes five figures, four movies and one table.

Supplementary Figure Legends

Figure S1. The structural changes of synapses at neuromuscular junctions (NMJs) of *PI31* $^{-/-}$ larva. Related to Figure 1 and Figure 7.

(A) The expression pattern of *R94G06-GAL4* illustrated by using it to drive *UAS-mCD8-mCherry*. (a) Brain and ventral nerve cord; **(b)** A single axon in nerve; **(c)** A NMJ at Muscle 1. Brp antibody (clone nc82, green) was used to visualize the synaptic neuropil regions. The results indicate that *R94G06-GAL4* is a specific driver for a subset of motor neurons (MN1-IB) targeting Muscle 1.

(B) Overview images for M4 NMJs of wild-type and *PI31*$^{-/-}$ larvae immunostained with anti-Brp (green) and anti-HRP (magenta) antibodies. It indicates that the overall morphology of NMJs is not dramatically changed, but the number of the core active zone (AZ) scaffold protein Brp puncta at NMJs is largely reduced in *PI31* $^{-/-}$ larvae. A high-magnification images of the boxed area are shown in Figure 1F, and quantification of Brp puncta is shown in Figure 1G.

(**C-D**) Representative images of NMJs at M6/7 indicate that the number of Brp puncta is largely reduced in *PI31* $^{-/-}$ larvae. **(C)** Overview images of M6/7 NMJs. **(D)** High-magnification images of the boxed area in (C). See quantification of Brp puncta in Figure 1G.

(**E**) Analysis of *PI31*$^{-/-}$ MARCM clones reveals that the reduction of Brp puncta is a neuron-autonomous phenotype. The GFP-positive neuron is *PI31*$^{-/-}$, whereas the GFP-negative neuron is *PI31*$^{+/-}$ (control). The control (*PI31*$^{+/-}$) and the *PI31*$^{-/-}$ M4 NMJs shown here were from the same larva. High-magnification images of the boxed regions are shown in Figure 1I, and quantification of Brp puncta is shown in Figure 1J.

Figure S2. DYNLL1/2 are binding partners of PI31. Related to Figure 2.

(A) Alignment of dDYNLL1/Ctp and dDYNLL2/Cdlc2. They differ in only one amino acid, which is highlighted by a pink box. The alignment was performed with Clustal Omega program on Uniprot server.

(B) The spectra of the unique peptides for dDYNLL1/Ctp (**a**, sequence: DIAAYIK) and dDYNLL2/Cdlc2 (**b**, sequence: DIAAFIK). The peptides were identified in the anti-HA-PI31 Co-IP samples using nano liquid chromatography and high-resolution MS. Both of them were matched with high confidence and with mass accuracy better than 0.5ppm. These results indicate that both proteins interact with PI31.

(C) Western blot analysis of anti-HA Co-IP experiments using protein extract of S2 cells expressing HA-PI31, indicating that PI31 interacts dDYNLL1/2 in S2 cells.

(D) Western blot analysis of anti-HA Co-IP experiments using protein extract of HEK293 cells expressing HA-hPI31, indicating that the interaction between PI31 and DYNLL1/2 is conserved in human cells.

Figure S3. Native gel analysis of PI31-bound complexes indicates that PI31 binds to both 20S and single-capped 26S proteasomes. Related to Figure 2.

HA-PI31$^{Knock\text{-}in}$ flies were collected, and anti-HA Co-IP experiments were conducted. The HA-PI31 and its interacting proteins were eluted by HA peptide under native conditions, and resolved on native gels. ATP was present during the Co-IP and native gel procedures. Anti-α7 and anti-Rpt3 antibodies that cross-react with respective *Drosophila* proteins were used for Western blot analysis to visualize 20S(α7), 19S(Rpt3) and 26S(both α7 and Rpt3) proteasomes. The results demonstrate that PI31 can bind to both 20S and single-capped 26S proteasomes, and may involve in their transport.

Figure S4. Generation of *PI31*^{S168A} *knock-in* fly strain. Related to Figure 7.

(A) Schematic diagram showing the sequence and position of the gRNA target site in the PI31 locus. UTRs are shown as gray blocks, and coding sequences are shown as dark red blocks. The codon for S168 is shown in red, whereas the PAM sequence is shown in blue. The Cas9 cut site is indicated by a yellow arrowhead.

(B) Partial DNA sequence of the HDR donor used to generate the S168A mutant. The codon for S168 is shown in red, whereas the PAM sequence is shown in blue. Besides the

S168A point mutation, we also introduced a silent mutation disrupting the PAM to avoid repeated cut by Cas9.

(C) The chromatogram obtained through Sanger sequencing of the PCR product amplified from a heterozygous fly. The arrows point out the positions of the S168A and PAM mutations. Double peaks represent an overlay of the sequences from the PI31S168A mutant and wild-type PI31 alleles. This result verified the precise integration of the donor DNA in the PI31 S168 position.

Figure S5. Generation and validation of pS153-hPI31 antibody. Related to Figure 8.

(A) Sequence of the phosphor-peptide used for the antibody generation. The phosphorylated residue is in red, and the N-terminal cysteine that is in green was added to facilitate the conjugation of the peptide to the carrier protein for immunization.

(B) Validation of the antibody specificity through the *in vitro* phosphatase assay. HA-hPI31 expressed in HEK293 cells were pulled down by anti-HA agarose beads, and treated with 400U lambda phosphatase at 30°C for 30 minutes with or without phosphatase inhibitors. The results indicate that the antibody recognized a clear band around 31kD, which was abolished by the phosphatase but rescued back by the phosphatase inhibitors. This data demonstrates that the pS153-hPI31 antibody specifically recognizes the phosphorylated hPI31.

Movie S1. A representative video of Prosβ5-RFP particle movement in an axon of a wild-type larva (*w; +/+; R94G06-GAL4, UAS-Prosβ5-RFP/R94G06-GAL4, UAS-Prosβ5-RFP*). Related to Figure 7. The video was acquired at 1.4Hz rate for 70 seconds (100 frames in total), and is shown in 10X of the original speed.

Movie S2. A representative video of Prosβ5-RFP particle movement in an axon of a *PI31*$^{-/-}$ larva (*w; PI31*$^{\Delta}$*/ PI31*$^{\Delta}$*; R94G06-GAL4, UAS-Prosβ5-RFP/R94G06-GAL4, UAS-Prosβ5-RFP*). Related to Figure 7. The video was acquired at 1.4Hz rate for 70 seconds (100 frames in total), and is shown in 10X of the original speed.

Movie S3. A representative video of Prosβ5-RFP particle movement in an axon of a

***PI31^{S168A} knock-in* larva (*w; PI31^{S168A} / PI31^{S168A}; R94G06-GAL4, UAS-Prosβ5-RFP/R94G06-GAL4, UAS-Prosβ5-RFP*). Related to Figure 7.** The video was acquired at 1.4Hz rate for 70 seconds (100 frames in total), and is shown in 10X of the original speed.

Movie S4. **A representative video of mCerulean-mPI31 (green) and α4-mCherry (red) movement in axons of cultured mouse DRG neurons. Related to Figure 7.** The video was acquired at 0.5Hz rate for 140 seconds (70 frames in total), and is shown in 10X of the original speed.

Table S1. Inactivation of PI31 in neurons results in an eclosion defect. Related to Figure 1.

Genotype	Eclosion rate
Nrv2-GAL4	98.5% (463/470)
UAS-PI31 RNAi	98.2% (163/166)
Nrv2>PI31 RNAi	0% (0/115)

Figure 1

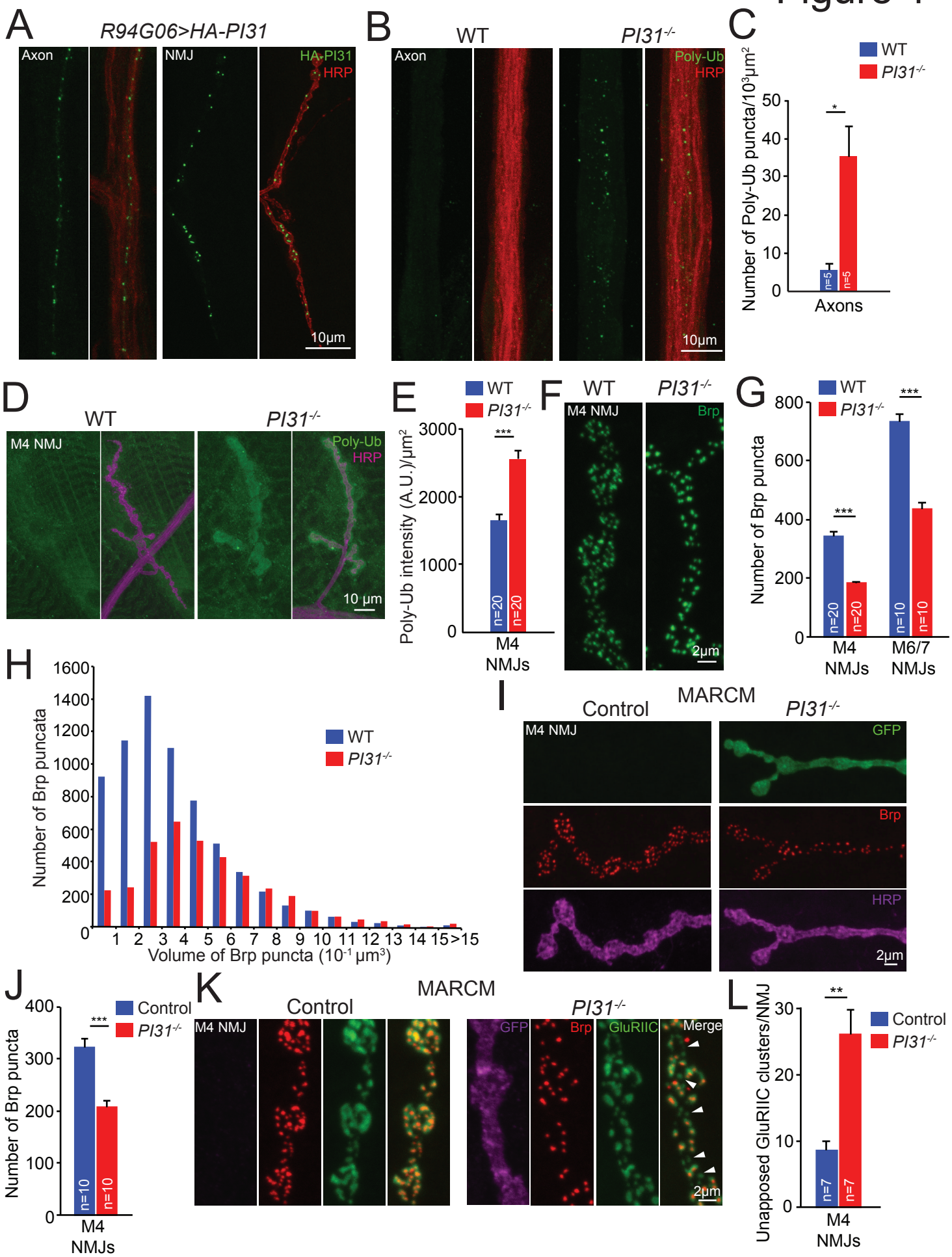
A
R94G06>HA-PI31
Axon
NMJ
HA-PI31
HRP
10µm
B
WT
PI31-/-
Axon
Poly-Ub
HRP
10µm
C
WT
PI31-/-
Number of Poly-Ub puncta/10³µm²
50
40
30
20
10
0
*
n=5
n=5
Axons
D
WT
PI31-/-
M4 NMJ
Poly-Ub
HRP
10 µm
E
WT
PI31-/-
Poly-Ub intensity (A.U.)/µm²
3000
2000
1000
0
***
n=20
n=20
M4
NMJs
F
WT
PI31-/-
M4 NMJ
Brp
2µm
G
WT
PI31-/-
Number of Brp puncta
800
600
400
200
0
***
***
n=20
n=20
n=10
n=10
M4
NMJs
M6/7
NMJs
H
Number of Brp puncata
1600
1400
1200
1000
800
600
400
200
0
WT
PI31-/-
1 2 3 4 5 6 7 8 9 10 11 12 13 14 15 >15
Volume of Brp puncta (10⁻¹ µm³)
I
MARCM
Control
PI31-/-
M4 NMJ
GFP
Brp
HRP
2µm
J
Control
PI31-/-
Number of Brp puncta
400
300
200
100
0
***
n=10
n=10
M4
NMJs
K
MARCM
Control
PI31-/-
M4 NMJ
GFP
Brp
GluRIIC
Merge
2µm
L
Control
PI31-/-
Unapposed GluRIIC clusters/NMJ
30
20
10
0
**
n=7
n=7
M4
NMJs

Figure 2

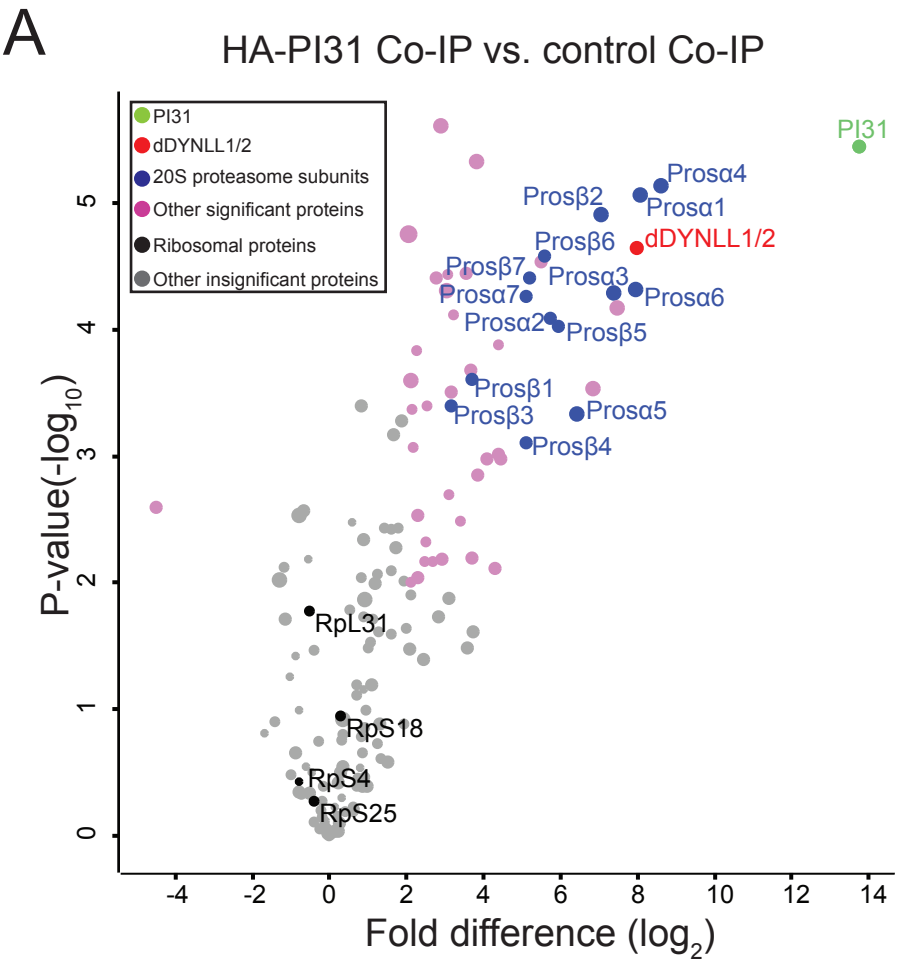
A
HA-PI31 Co-IP vs. control Co-IP
PI31
dDYNLL1/2
20S proteasome subunits
Other significant proteins
Ribosomal proteins
Other insignificant proteins
PI31
Prosα4
Prosβ2
Prosα1
Prosβ6
dDYNLL1/2
Prosβ7
Prosα3
Prosα7
Prosα6
Prosα2
Prosβ5
Prosβ1
Prosα5
Prosβ3
Prosβ4
RpL31
RpS18
RpS4
RpS25
P-value(-log10)
Fold difference (log2)

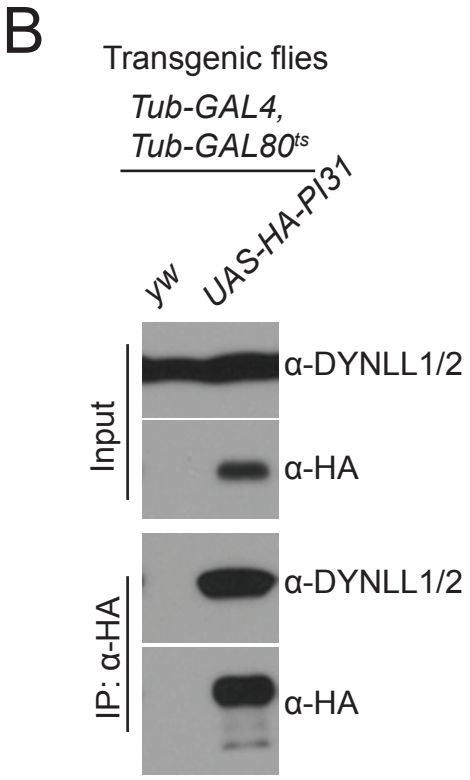
B
Transgenic flies
Tub-GAL4,
Tub-GAL80ts
yw
UAS-HA-PI31
Input
α-DYNLL1/2
α-HA
IP: α-HA
α-DYNLL1/2
α-HA

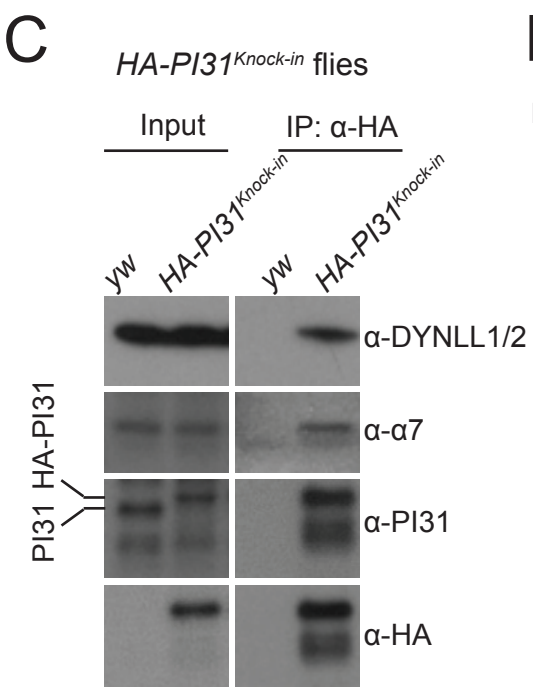
C
HA-PI31Knock-in flies
Input
IP: α-HA
yw
HA-PI31Knock-in
yw
HA-PI31Knock-in
α-DYNLL1/2
α-α7
PI31 HA-PI31
α-PI31
α-HA

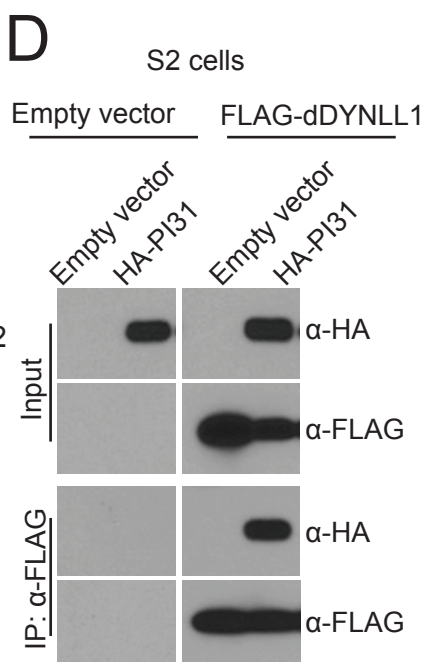
D
S2 cells
Empty vector
FLAG-dDYNLL1
Empty vector
HA-PI31
Empty vector
HA-PI31
Input
α-HA
α-FLAG
IP: α-FLAG
α-HA
α-FLAG

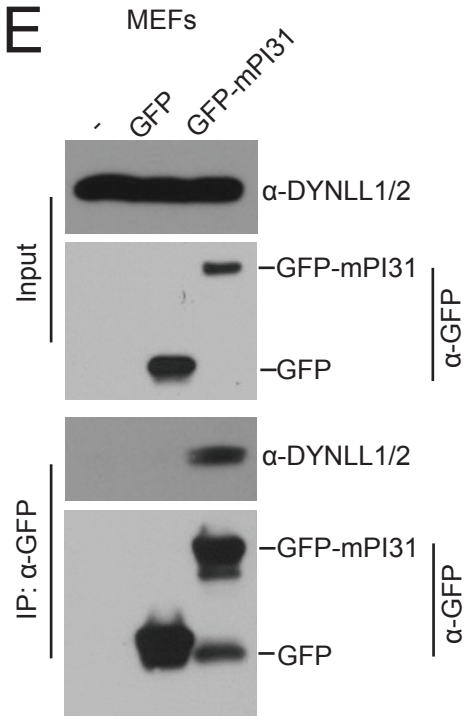
E
MEFs
-
GFP
GFP-mPI31
Input
α-DYNLL1/2
GFP-mPI31
GFP
α-GFP
IP: α-GFP
α-DYNLL1/2
GFP-mPI31
GFP
α-GFP

Figure 3

A

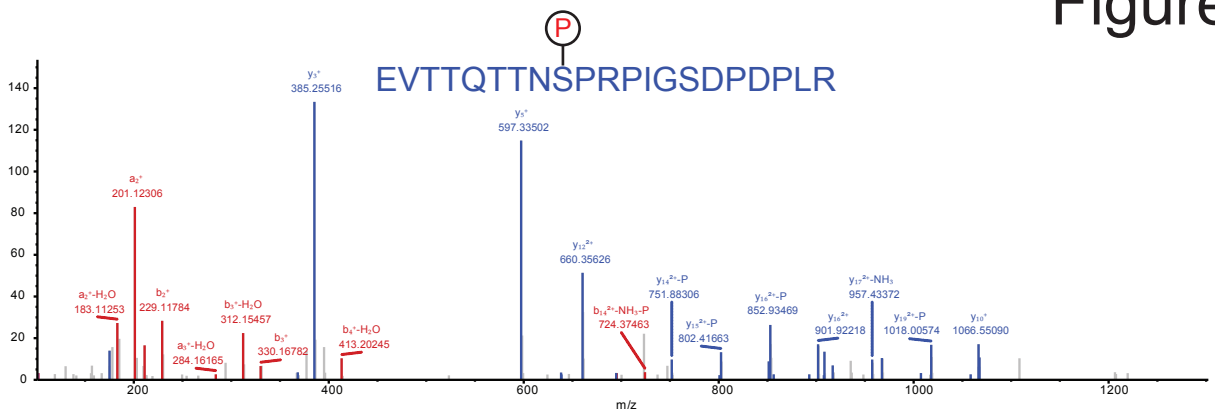

B

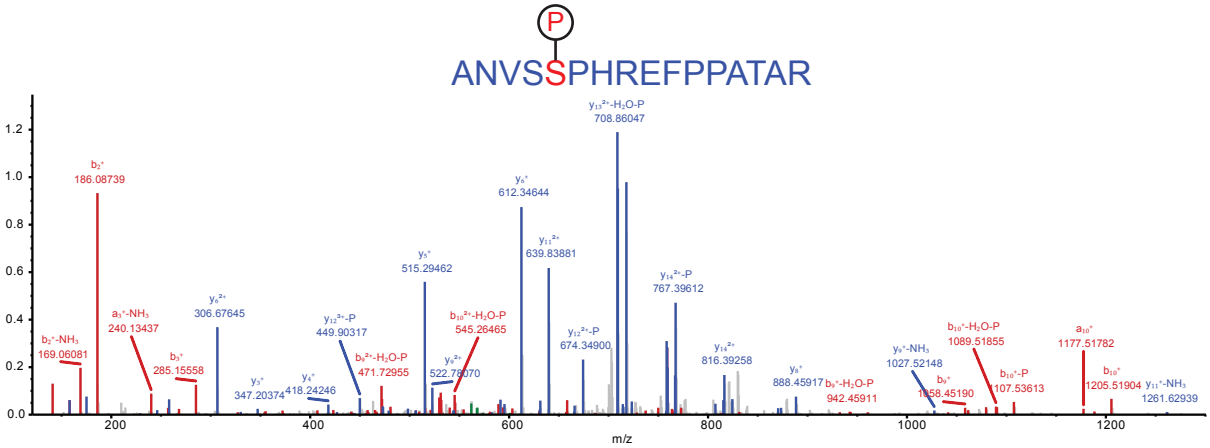

C

D

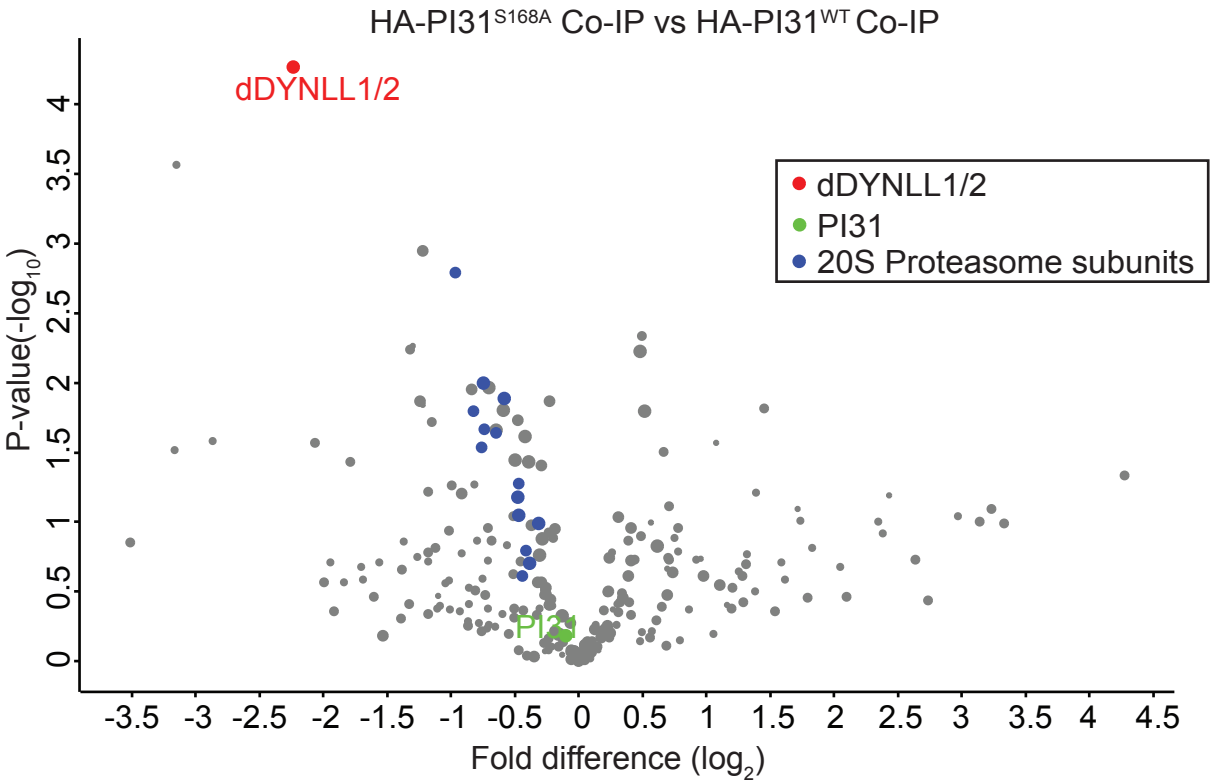

Figure 4

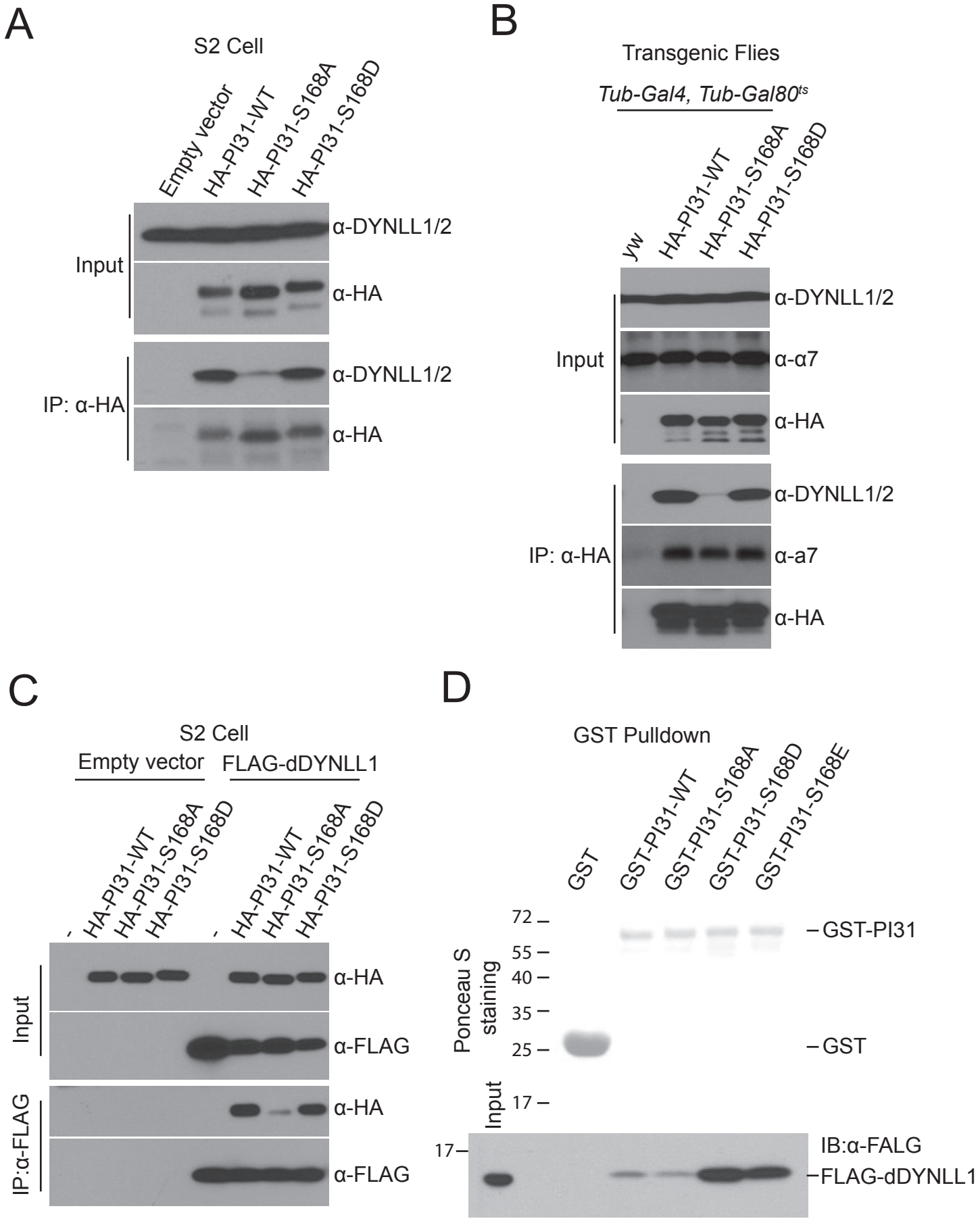
A
S2 Cell
Empty vector
HA-PI31-WT
HA-PI31-S168A
HA-PI31-S168D
Input
IP: α-HA
α-DYNLL1/2
α-HA
α-DYNLL1/2
α-HA
B
Transgenic Flies
Tub-Gal4, Tub-Gal80ts
yw
HA-PI31-WT
HA-PI31-S168A
HA-PI31-S168D
Input
IP: α-HA
α-DYNLL1/2
α-α7
α-HA
α-DYNLL1/2
α-a7
α-HA
C
S2 Cell
Empty vector
FLAG-dDYNLL1
-
HA-PI31-WT
HA-PI31-S168A
HA-PI31-S168D
Input
IP:α-FLAG
α-HA
α-FLAG
α-HA
α-FLAG
D
GST Pulldown
GST
GST-PI31-WT
GST-PI31-S168A
GST-PI31-S168D
GST-PI31-S168E
Ponceau S staining
72
55
40
35
25
17
GST-PI31
GST
Input
17
IB:α-FALG
FLAG-dDYNLL1

Figure 5

A

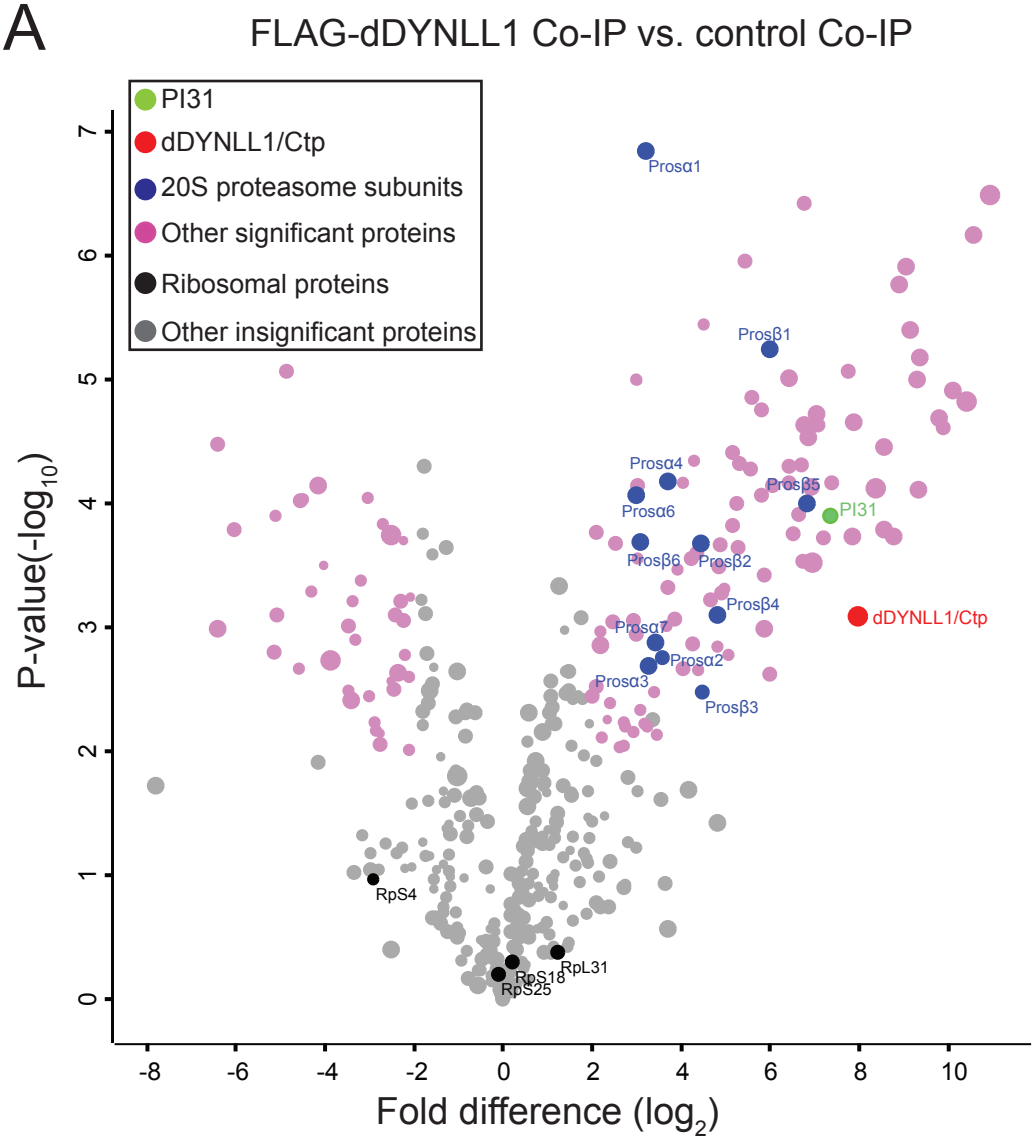
FLAG-dDYNLL1 Co-IP vs. control Co-IP
PI31
dDYNLL1/Ctp
20S proteasome subunits
Other significant proteins
Ribosomal proteins
Other insignificant proteins
Prosα1
Prosβ1
Prosα4
Prosβ5
Prosα6
PI31
Prosβ6
Prosβ2
Prosβ4
dDYNLL1/Ctp
Prosα7
Prosα2
Prosα3
Prosβ3
RpS4
RpL31
RpS18
RpS25
P-value(-log10)
Fold difference (log2)
-8
-6
-4
-2
0
2
4
6
8
10
0
1
2
3
4
5
6
7

B

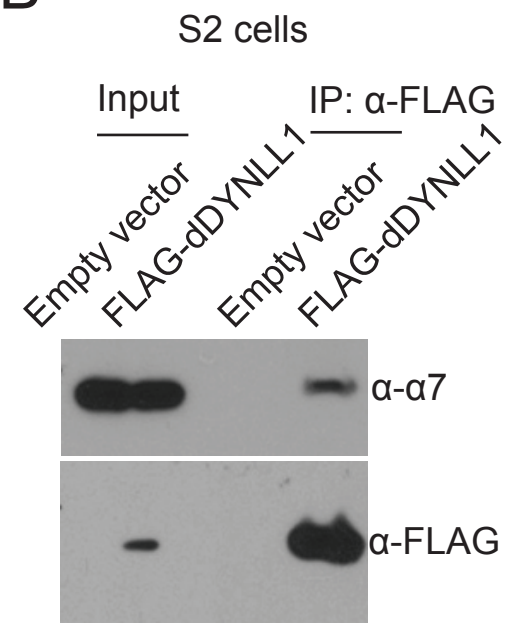
S2 cells
Input
IP: α-FLAG
Empty vector
FLAG-dDYNLL1
Empty vector
FLAG-dDYNLL1
α-α7
α-FLAG

Figure 6

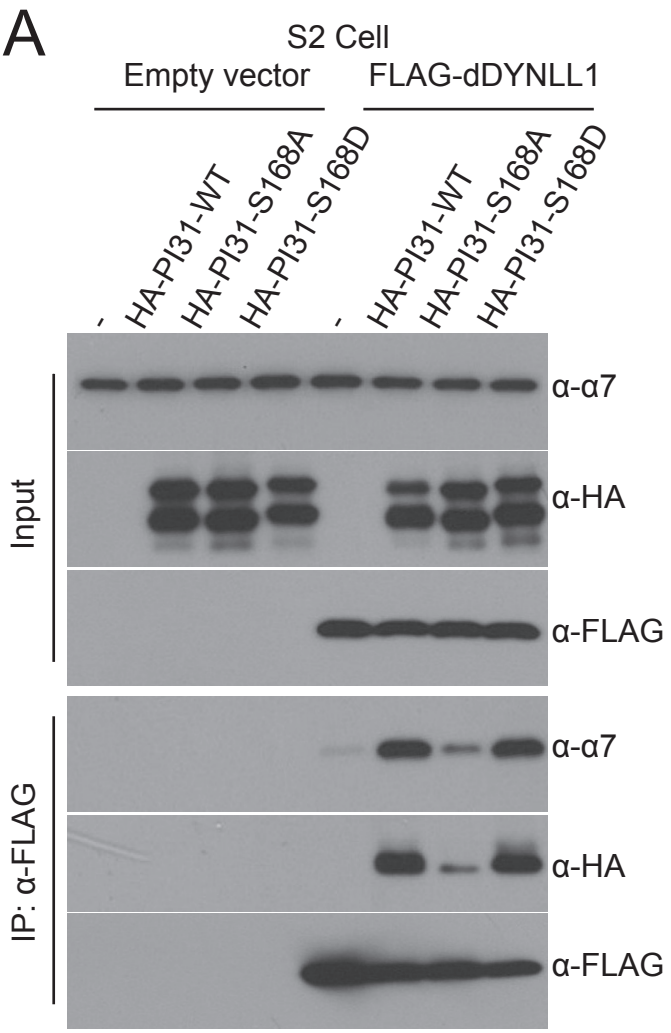
A
S2 Cell
Empty vector
FLAG-dDYNLL1
-
HA-PI31-WT
HA-PI31-S168A
HA-PI31-S168D
-
HA-PI31-WT
HA-PI31-S168A
HA-PI31-S168D
Input
IP: α-FLAG
α-α7
α-HA
α-FLAG
α-α7
α-HA
α-FLAG

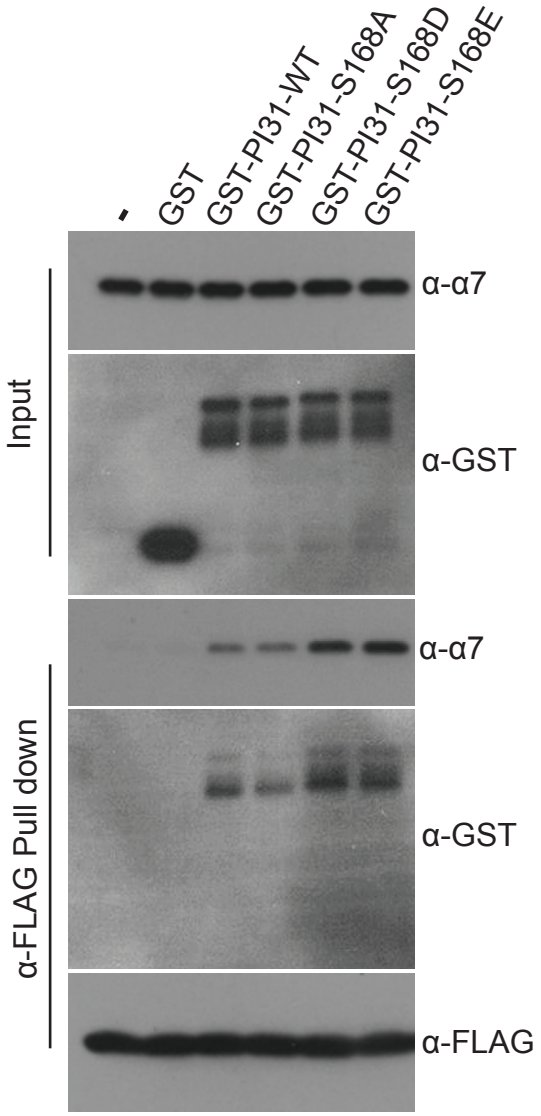
B
In vitro reconstitution
Beads
dDYNLL1
GST
GST -PI31
-
GST
GST-PI31-WT
GST-PI31-S168A
GST-PI31-S168D
GST-PI31-S168E
Input
α-α7
α-GST
α-α7
α-GST
α-FLAG
α-FLAG Pull down

Figure 7

A

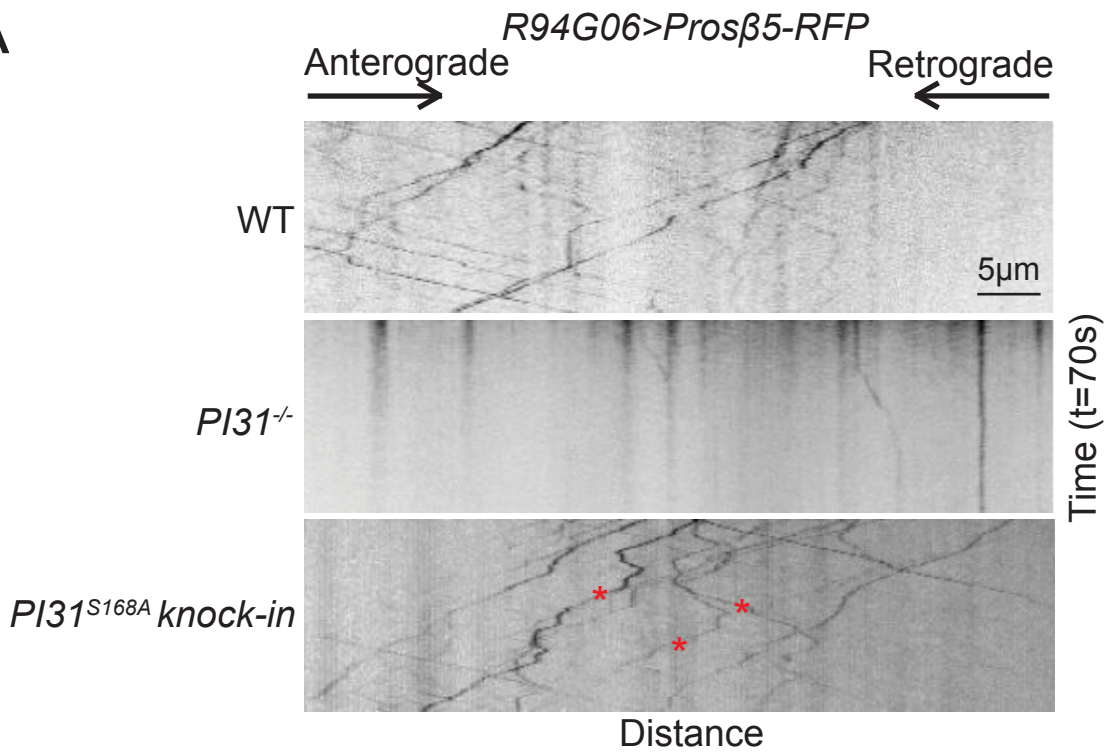

B

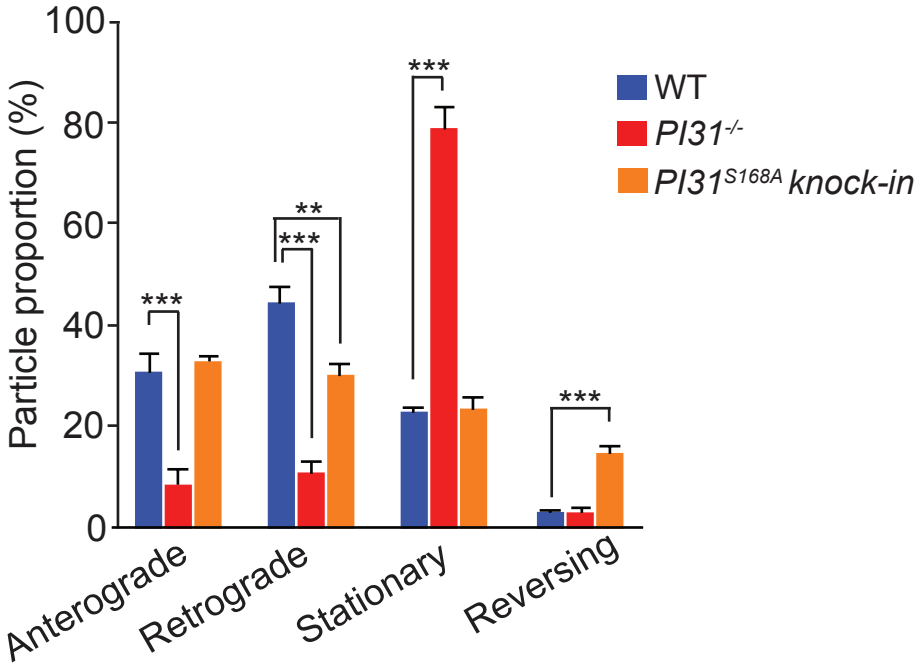

C

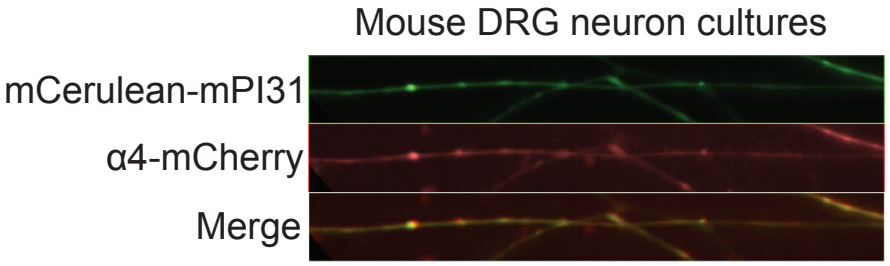

D

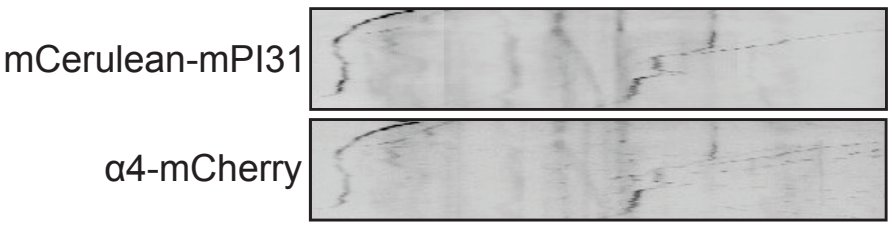

Figure 8

A

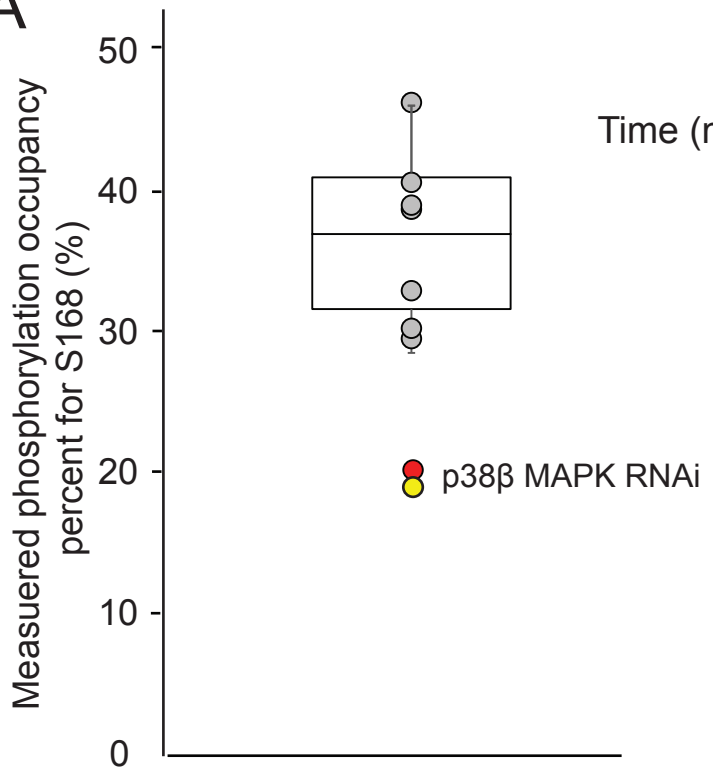

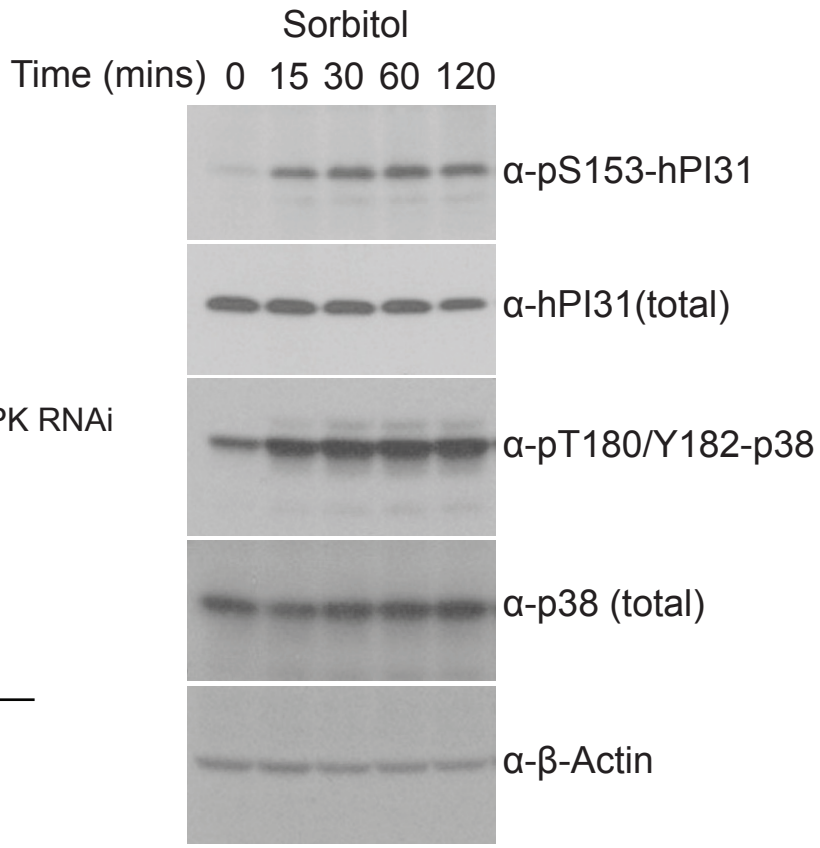

C

Sorbitol	-	+	+	+	+
DMSO	+	+	-	-	-
SB203580	-	-	+	-	-
SB202190	-	-	-	+	-
BIRB796	-	-	-	-	+

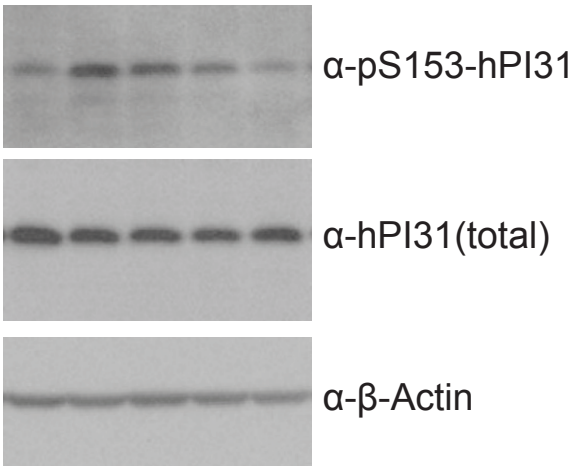

D

In vitro kinase assay

hPI31	+	+	+	+	+
GST-p38α	-	+	-	-	-
His-p38β	-	-	+	-	-
His-p38γ	-	-	-	+	-
His-p38δ	-	-	-	-	+

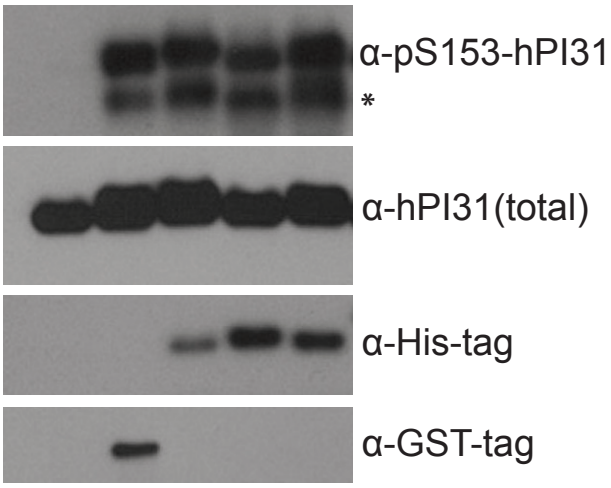

Figure 9

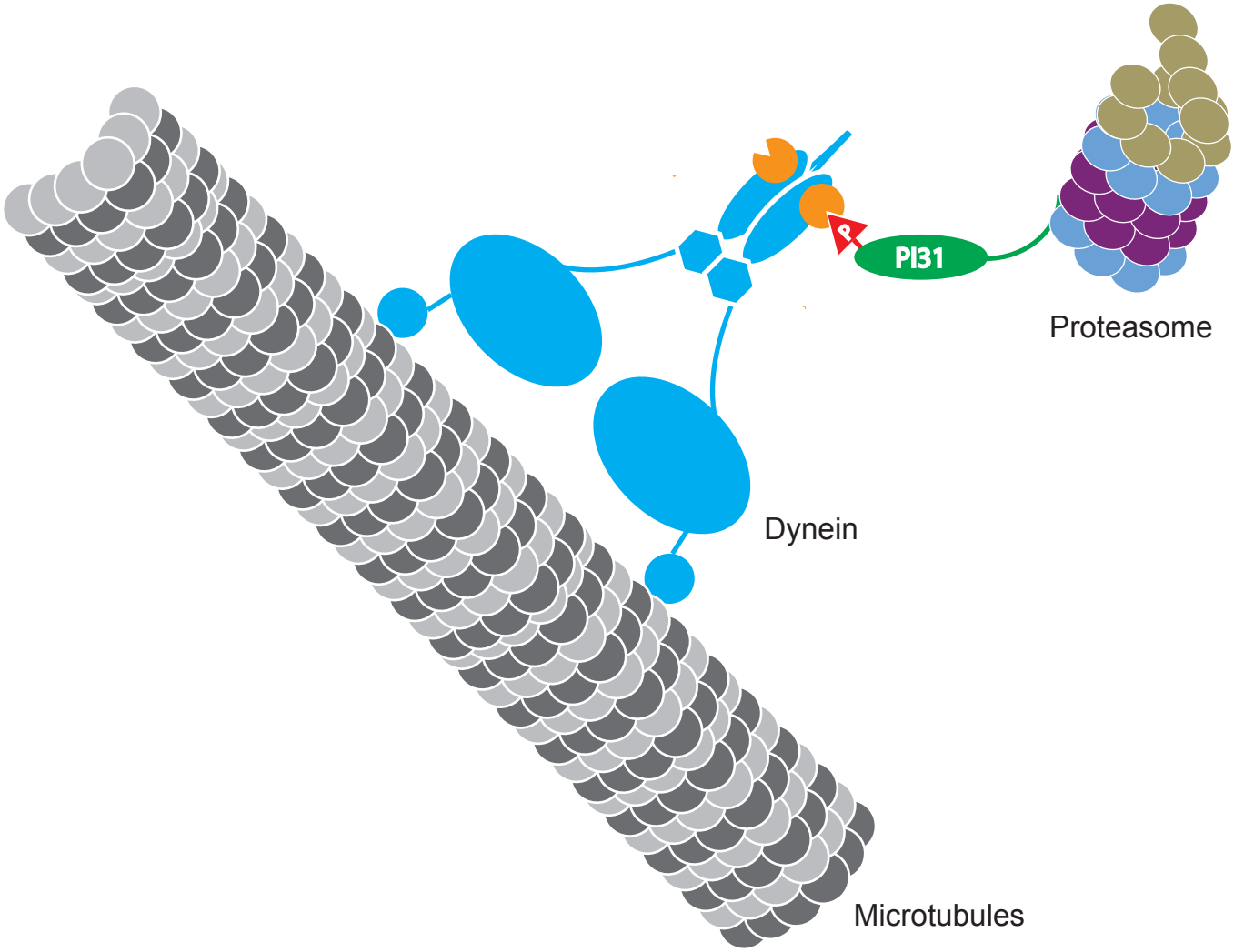

Figure S1

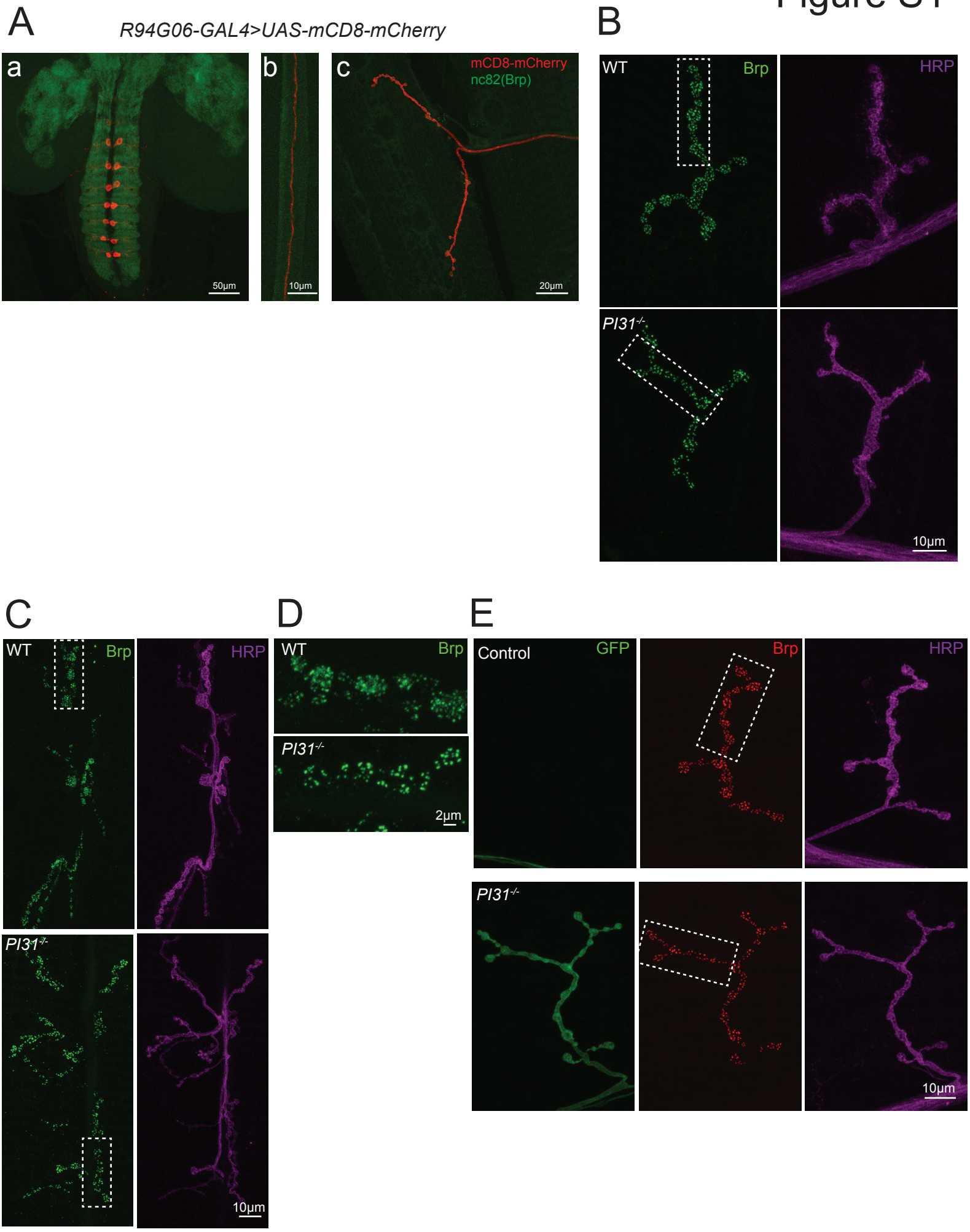
A
R94G06-GAL4>UAS-mCD8-mCherry
a
50μm
b
10μm
c
mCD8-mCherry
nc82(Brp)
20μm
B
WT
Brp
HRP
PI31-/-
10μm
C
WT
Brp
HRP
PI31-/-
10μm
D
WT
Brp
PI31-/-
2μm
E
Control
GFP
Brp
HRP
PI31-/-
10μm

Figure S2

A

```
dDYNLL1/Ctp     MSDRKAVIKNADMSEEMQQDAVDCATQALEKYNIEKDIAAYIKKEFDKKYNPTWHCIVGRNFGSYVTHETRHFIYFYLGQVAILLFKSG
dDYNLL2/Cdlc2   MSDRKAVIKNADMSEEMQQDAVDCATQALEKYNIEKDIAAFIKKEFDKKYNPTWHCIVGRNFGSYVTHETRHFIYFYLGQVAILLFKSG
                ****************************************:***************************************************
```

B

a

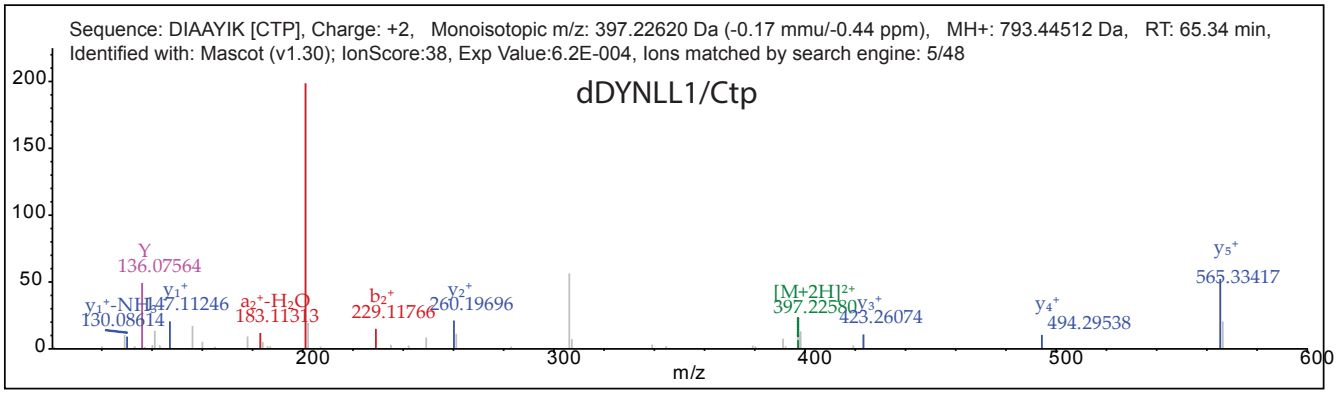

b

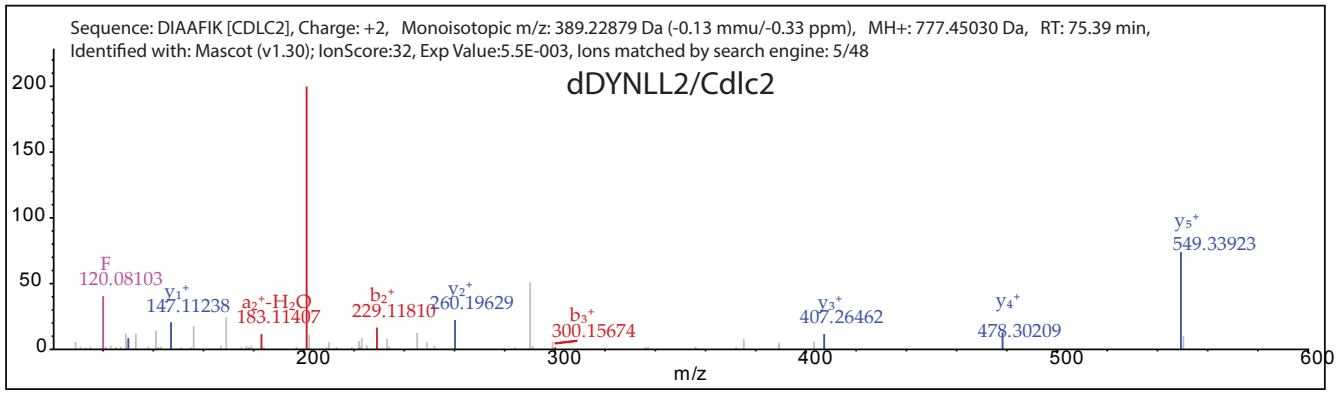

C

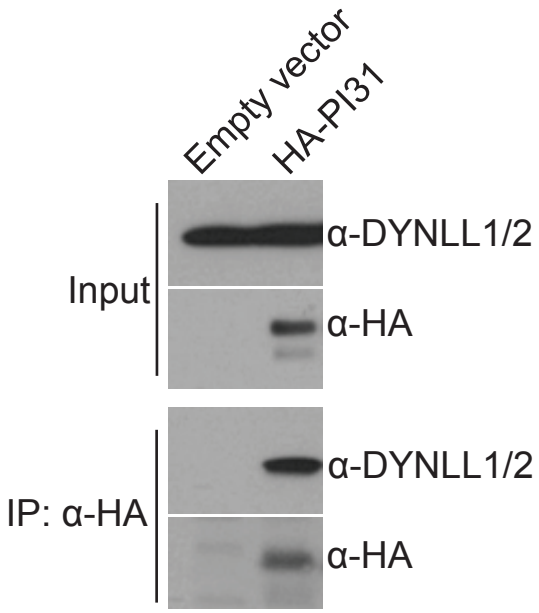

D

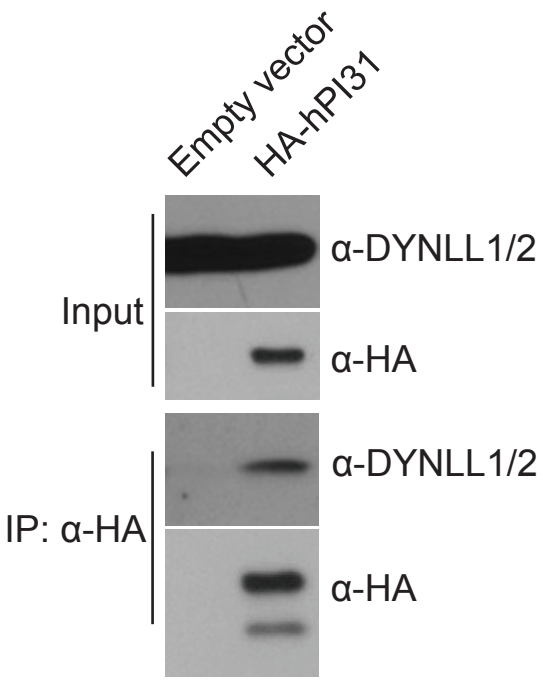

Figure S3

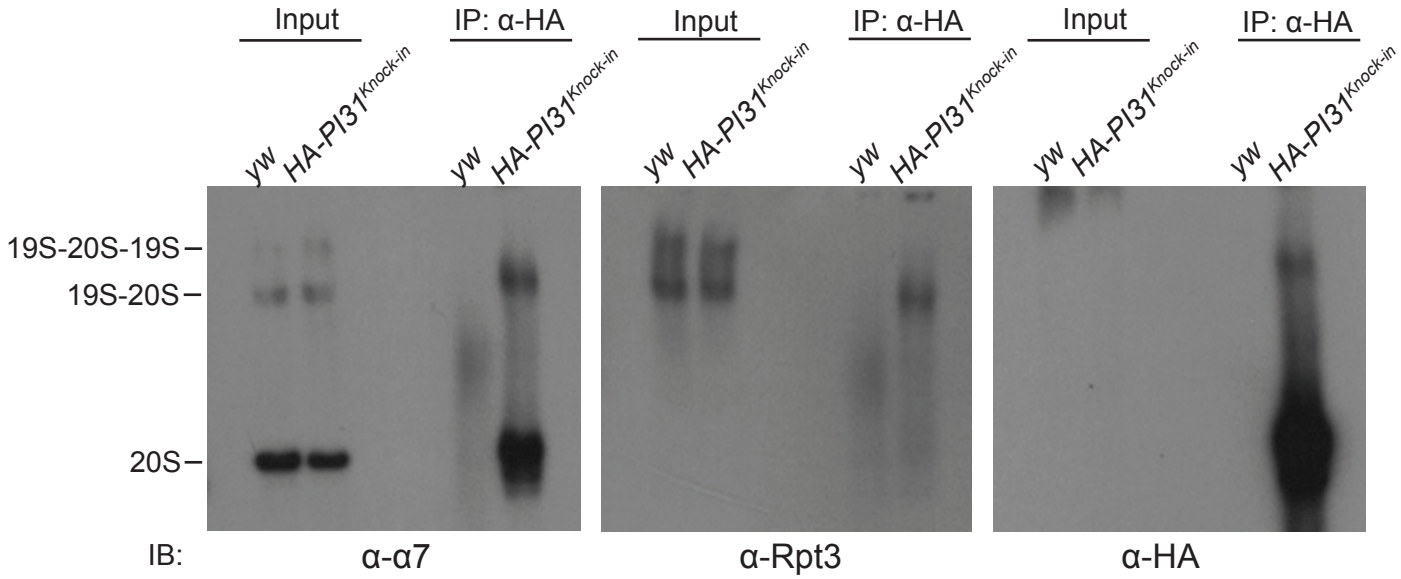
Input
IP: α-HA
Input
IP: α-HA
Input
IP: α-HA
yw
HA-PI31Knock-in
yw
HA-PI31Knock-in
yw
HA-PI31Knock-in
yw
HA-PI31Knock-in
yw
HA-PI31Knock-in
yw
HA-PI31Knock-in
19S-20S-19S
19S-20S
20S
IB:
α-α7
α-Rpt3
α-HA

Figure S4

A

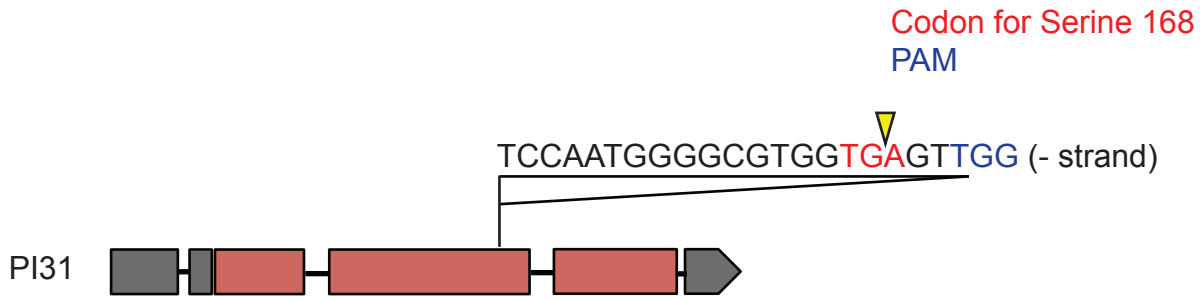

B

Donor sequence

WT	---TCCAATGGGGCGTGGTGAGTTGG---
S168A	---TCCAATGGGGCGTGGTGCGTTCG---

C

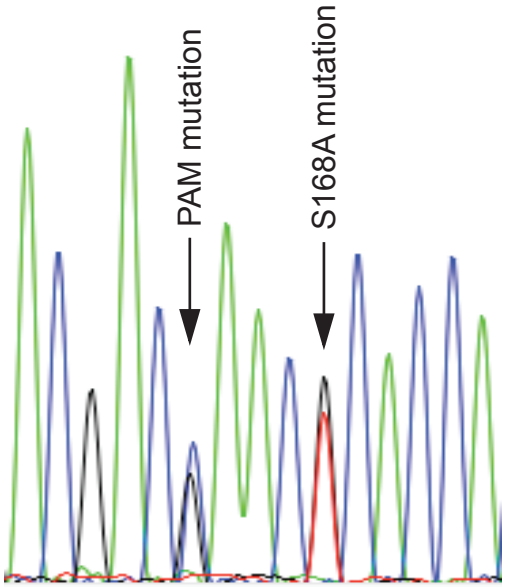

Figure S5

A

Phospho-peptide used for generating pS153-hPI31 specific antiboy

hPI31 146-159

CWEKANVSpSPHREFP-amide

B
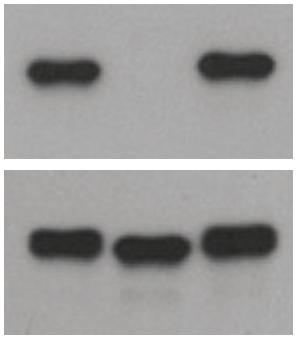
Phosphatase	-	+	+
Phosphatase inhibitor	-	-	+